**Non-canonical adrenergic neuromodulation of motoneuron intrinsic excitability through β-receptors in wild-type and ALS mice**

*Stefano Antonucci[1], *Guillaume Caron[2], Natalie Dikwella[1], Sruthi Sankari Krishnamurty [1], Hina Zarrin[1], Aboud Tahanis[1], Florian Olde Heuvel[1], Simon M. Danner[4], Albert Ludolph[1,3], Kamil Grycz[5], **Marcin Baczyk[5], **Daniel Zytnicki[2], **Francesco Roselli[1,3]

Affiliations: 1) Dept. of Neurology, Ulm University, Ulm, DE.
2) Université Paris Cité, CNRS, Saints-Pères Paris Institute for the Neurosciences, Paris, France.
3) German Center for Neurodegenerative Diseases (DZNE)-Ulm, DE
4) Department of Neurobiology and Anatomy, College of Medicine, Drexel University, Philadelphia, United States.
5) Dept. of Neurobiology, Poznan University of Physical Education, Poland

*equal contribution
** co-senior authors

Corresponding authors: prof. dr. Francesco Roselli,
Center for Biomedical Research (ZBF)
Helmholtzstrasse 8/1-89081 Ulm DE
phone: 0049 0731 500 63147
email: francesco.roselli@uni-ulm.de

prof. dr. Daniel Zytnicki,
Université Paris Cité
Saints-Pères Paris Institute for the Neurosciences,
45 rue des Saints-Pères, F-75006 Paris
email: daniel.zytnicki@u-paris.fr

prof. dr. Marcin Bączyk,
Poznan University of Physical Education.
Krolowej Jadwigi 27/39, 60-871 Poznan, Poland
email: baczyk@awf.poznan.pl

Key words:
Spinal motoneurons, adrenergic neuromodulation, GPCR, PKA pathway, Amyotrophic Lateral Sclerosis, transcriptomics, *in vivo* electrophysiology.

**Summary**

Altered neuronal excitability and synaptic inputs to motoneurons are part of the pathophysiology of Amyotrophic Lateral Sclerosis. The cAMP/PKA pathway regulates both of them but therapeutic interventions at this level are limited by the lack of knowledge about suitable pharmacological entry points. Here we used transcriptomics on microdissected and *in situ* motoneurons to reveal the modulation of PKA-coupled receptorome in SOD1(G93A) ALS mice, vs WT, demonstrating the dysregulation of multiple PKA-coupled GPCRs, in particular on vulnerable MNs, and the relative sparing of β-adrenergic receptors. *In vivo* MN electrophysiology showed that β2/β3 agonists acutely increase excitability, in particular the input/output relationship, demonstrating a non-canonical adrenergic neuromodulation mediated by β2/β3 receptors both in WT and SOD1 mice. The excitability increase corresponds to the upregulation of immediate-early gene expression and dysregulation of ion channels transcriptome. However the β2/β3 neuromodulation is submitted to a strong homeostasis, since a ten days delivery of β2/β3 agonists results in an abolition of the excitability increase. The homeostatic response is largely caused by a substantial downregulation of PKA-coupled GPCRs in MNs from WT and SOD1 mice. Thus, β-adrenergic receptors are physiologically involved in the regulation of MN excitability and transcriptomics, but, intriguingly, a strong homeostatic response is triggered upon chronic pharmacologic intervention.

## Introduction

Firing properties of spinal motoneurons (MNs) can be dynamically modified through neuromodulation of currents that contribute to MN excitability (Reckling *et al*., 2000, Heckman *et al*., 2009). Although the full extent of neuromodulatory inputs has not yet been systematically investigated (Heckman *et al*., 2009), monoaminergic modulators deeply affect the excitability of spinal MNs. Serotonin increases MN excitability through 5-$HT_2$ receptors and conversely reduces firing through 5-$HT_{1A}$ receptors (Perrier 2019, Reckling *et al*., 2000). Dopamine was reported to increase intrinsic excitability of spinal MN in neonate mice (Han *et al*., 2007) whereas D1-like receptors, but not D2-like, were found to increase AMPA currents (Han and Whelan 2009). Noradrenaline was also reported to have many effects on MN excitability through α receptors, mainly α1 (Reckling *et al*., 2000). To our knowledge, a single work has reported a role for β1 receptors in neonate rats : it decreases the F-I gain of MNs at this age (Tartas *et al*., 2010). However, β2/β3 receptors have never been shown yet to modulate MN excitability.

Nevertheless, β-adrenergic receptors display a substantial translational potential. A large number of β-adrenergic agonists and antagonists is well-characterized in clinical practice (Michel and Balligand, 2017; Matera *et al*., 2020) and pathological alterations of MN excitability and firing characterize multiple spinal cord diseases (Nielsen *et al*., 2007; Baczyk *et al*., 2022). Therefore, elucidation of β-adrenergic receptors neuromodulatory properties is highly relevant in the framework of their utilization as a therapeutic entry-point.

In particular, Amyotrophic Lateral Sclerosis (ALS) is characterized by alterations in the firing pattern of MNs. In a murine model of ALS, the SOD1(G93A) ALS murine model, mice (henceforth SOD1), hyperexcitable MNs can be found in juvenile animals (P6-P10) (Leroy *et al*., 2014) whereas in presymptomatic adult animals (P45-P59) the largest MNs (innervating FF and FR motor units) become unable to fire repetitively in response to a sustained stimulus (Delestrée *et al*., 2014, Martinez-Silva *et al*., 2018). These MN subtypes are the most vulnerable in ALS, raising the possibility of a link between the loss of firing and the early degeneration.

In fact, modulation of MN excitation through either chemogenetics *in vivo* ALS model (Saxena *et al*., 2013) or through $K^+$ blockers in in vitro systems (Catanese *et al*., 2021; Naujock *et al*., 2016) has been shown to positively affect disease pathways; thus, interventions aimed at modulating MN physiological properties may have therapeutic value in ALS. In this direction, β-adrenergic receptors are of interest also because of their Gs/cAMP/PKA signaling. In fact, a chemogenetic activation of the cAMP/PKA pathway by DREADD(Gs) system was found to reduce the MN burden of the disease markers and partially restore the integrity of excitatory synapses (Baczyk *et al*., 2020). Furthermore, enhancing the cAMP signaling reduced disease markers in a poly-GA ALS in vitro model (Khosravi *et al*., 2020).

Since modulation of MN excitability as well as the activation of the cAMP/PKA pathway proved to be neuroprotective to presymptomatic ALS MNs, we investigated if GPCRs may be suitable entry points to obtain neuromodulation of MN physiology through cAMP/PKA activation. We found that β-adrenergic receptors are highly expressed in MNs and relatively spared in ALS MNs. We then demonstrated that human-approved β2/β3 agonists engage the PKA pathway, elicit immediate-early genes and ion channel transcriptional regulation and acutely increase MN firing and excitability, demonstrating a non-canonical pathway for the adrenergic neuromodulation. Thereby, we show that β2 and β3 receptors are new players that provide neuromodulation of MN firing in both WT and SOD1 mice. However, chronic β2/β3 receptors agonists administration elicits a strong homeostatic downregulation of their own expression and of MN excitability both in WT and SOD1 mice, negating the excitability increase observed upon acute administration.

## Results

1. *Differential expression of the cAMP/PKA receptorome in MNs of WT and ALS mice*

We established a screening pipeline based on available datasets to identify PKA-coupled GPCRs expressed in MNs and with high translational potential. Out of the >400 mammalian GPCRs listed in the GPCRdb database (Kooistra *et al*., 2021), we extracted the subgroup affecting the cAMP/PKA signaling (i.e., either Gs- or Gi-coupled) and out of these we annotated those expressed in MNs according to the Allen Spinal Cord Atlas (Henry and Hohmann, 2012). The resulting priority set (30 GPCRs from 12 families) included dopaminergic, β-adrenergic, histaminergic receptors

together with receptors for adenosine, opioids and several lipid mediators and neuropeptides. Notably, the role of most of these receptors in MN physiology and biology is unknown.

We probed the expression of the prioritized GPCR set at P45 (presymptomatic stage; Martinez-Silva *et al*., 2018; Baczyk *et al*., 2020) in lumbar MNs from SOD1 and WT animals isolated by laser-capture-microdissection (LCM; 30 MNs > 500 $\mu m^2$ from L4-L5, as in Song *et al*., 2023). Unsupervised hierarchical clustering (Fig. 1A) and subsequent t-tests identified a significant genotype effect: 9/30 GPCRs were downregulated in SOD1 MNs (Fig. 1A; *Oprd1*, *Adora2b*, *Bdkrb1*, *Drd5*, *Chrm2*, *Adrb2*, *Gpr68, Drd2, Hrh3),* 10/30 were upregulated (Fig. 1A, C; *Gpr65*, *Grm8*, *Cckar*, *Gabbr2*, *Adrb1*, *Grm4*, *Hcar2*, *Atgr1a*, *Gpr3* and *Chrm4*) and 11/30 GPCR (Fig. 1A; *Adcyap1r1, Hcar1*, *Oprl1*, *Pthr1*, *Htr7*, *Adrb3*, *P2ry12*, *Lpar4*, *S1pr5, Tacr1* and *Adora2a*) were comparably expressed. Notably, the β-adrenergic receptors (*Adrb1-3*) were highly expressed in MNs and either upregulated (*Adrb1*) or downregulated (*Adrb2*) or unmodified (*Adrb3*) in ALS MNs (Fig. 1B-G). Because of the high translational value (small-molecule agonists and antagonists are approved for human use) and the limited understanding of their physiological role, we focused on this receptor family for further characterization.

We set out to validate the expression pattern of *Adrb1-3* by single-molecule *in situ* hybridization (SM-ISH), distinguishing MN subtypes according to *Mmp9* expression (*Mmp9*+ MNs are disease-vulnerable FF and large FR MNs whereas *Mmp9*- MNs are disease-resistant small FR and S; Kanning *et al*., 2010; Kaplan *et al*., 2014; Leroy *et al*., 2014). *Adrb1-3* mRNA was more abundant in *Mmp9*+ than in *Mmp9*- MNs (50% or fewer mRNA molecules in *Mmp9*- MNs; Fig. 1B-G). Nevertheless, the disease-related modulation was largely (but not completely) similar in the two subpopulations: *Adrb1* was upregulated only in *Mmp9*+ MNs (Fig. 1B-C) whereas *Adrb2* (Fig. 1D-E) and *Adrb3* (Fig. 1F-G) were unmodified in both subpopulations. We also validated the expression of four more GPCRs (*Hrh3, Adora2b*, *Chrm2* and *Drd5*) by SM-ISH (Supplemental Fig. 1A-H). The differential expression pattern of these GPCRs was largely in agreement with the LCM data (with the exception of *Drd5*; Supplemental Fig. 1G-H).

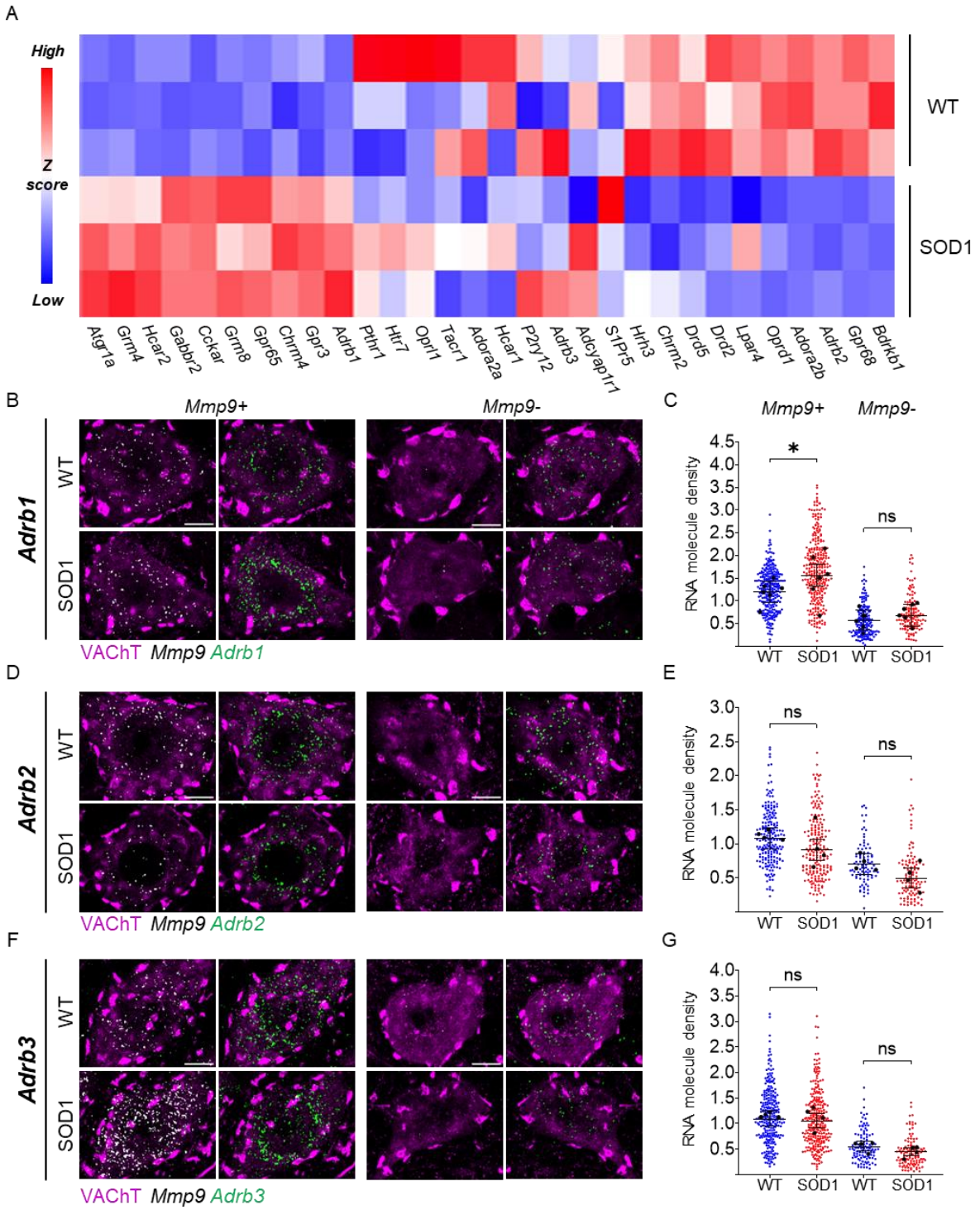


**Figure 1 | Expression patterns of PKA-coupled GPCR in ALS MNs. A) GPCR-targeted transcriptomics in laser-microdissected MNs reveals distinct up- and downregulation patterns** (p45 SOD1 and WT MNs; *blue*, downregulated genes; *red*, upregulated genes; 30 MNs per animal, n=3 animals. **B-C)** Single-molecule in situ mRNA hybridization confirms the upregulation of *Adrb1* mRNA in *Mmp9+* (vulnerable), but not in *Mmp9-* (resistant) MNs. **D-G)** ISH reveals the comparable expression of *Adrb2* (D-E) and *Adrb3* (F-G) in WT and SOD1 MNs. Expression levels are quantified as the number of mRNA molecules per unit area. Scatterplots depict individual MNs (small dots) and average expression per animal (large black dots); bars represent mean and 95% confidence intervals. N = 4-7 mice per group. *p<0.05, **p<0.01, ***p<0.001, ****p<0.0001.

2. *β2 and β3 agonists activate PKA signaling, induce immediate-early genes and modulate ion channels*

Preliminarily to physiological and functional studies, we demonstrated the ability of two FDA-approved adrenergic β2 and β3 agonists (formoterol and amibegron, respectively) to engage signal transduction and modulate gene expression in MNs. WT or SOD1 mice were administered β2/β3 agonists (or vehicle) and PKA cascade activation was assessed at 3h in spinal cord sections by immunolabeling for the PKA-phosphorylated consensus motif RRxpS/T. At baseline (vehicle-treatment), SOD1 MNs displayed a lower RRxpS/T immunostaining than WT (Fig.2A); however, agonist treatment elicits a substantial increase in RRxpS/T immunoreactivity (Fig. 2A), indicating target engagement (increased in RRxpS/T immunoreactivity was also observed in vasculature; Fig. 2A).

Next, we demonstrated MN transcriptional responses induced by β2/β3 adrenergic receptors. In LCM MNs, β2/β3 adrenergic agonists upregulated the expression of multiple immediate-early genes both in WT and SOD1 animals (3h after treatment; in particular, cFos, ΔFosB, Egr1, Npas4 were induced in WT animals and Fos, ΔFosB, in SOD1; Fig. 2B) as well as Egr2 and Arc (see Supplemental Excel Table 1). Finally, we explored the potential neuromodulatory effects of β2/β3 stimulation by assessing its impact on the expression of 19 $K^+$, $Na^+$, $Ca^{2+}$, $Cl^-$ and non-selective cation channels. Three hours after β2/β3 agonists administration, the majority of considered channels were significantly modulated (down- or up-regulated) both in WT and SOD1 MNs (Fig. 2C). Notably, the PCA analysis of the ion channel transcriptomes revealed the clear distinction of both vehicle and β2/β3 MNs, with the PC1 (42.7% of the variability) representing the effect of adrenergic stimulation.

Taken together, these data demonstrate that β2/β3 receptors on MNs are engaged by agonists and linked to signaling and transcriptional responses. Since the functional effects of β2/β3 receptors cannot be inferred solely from transcriptional data, we proceeded to exploit *in vivo* electrophysiology for the characterization of their neuromodulatory properties.

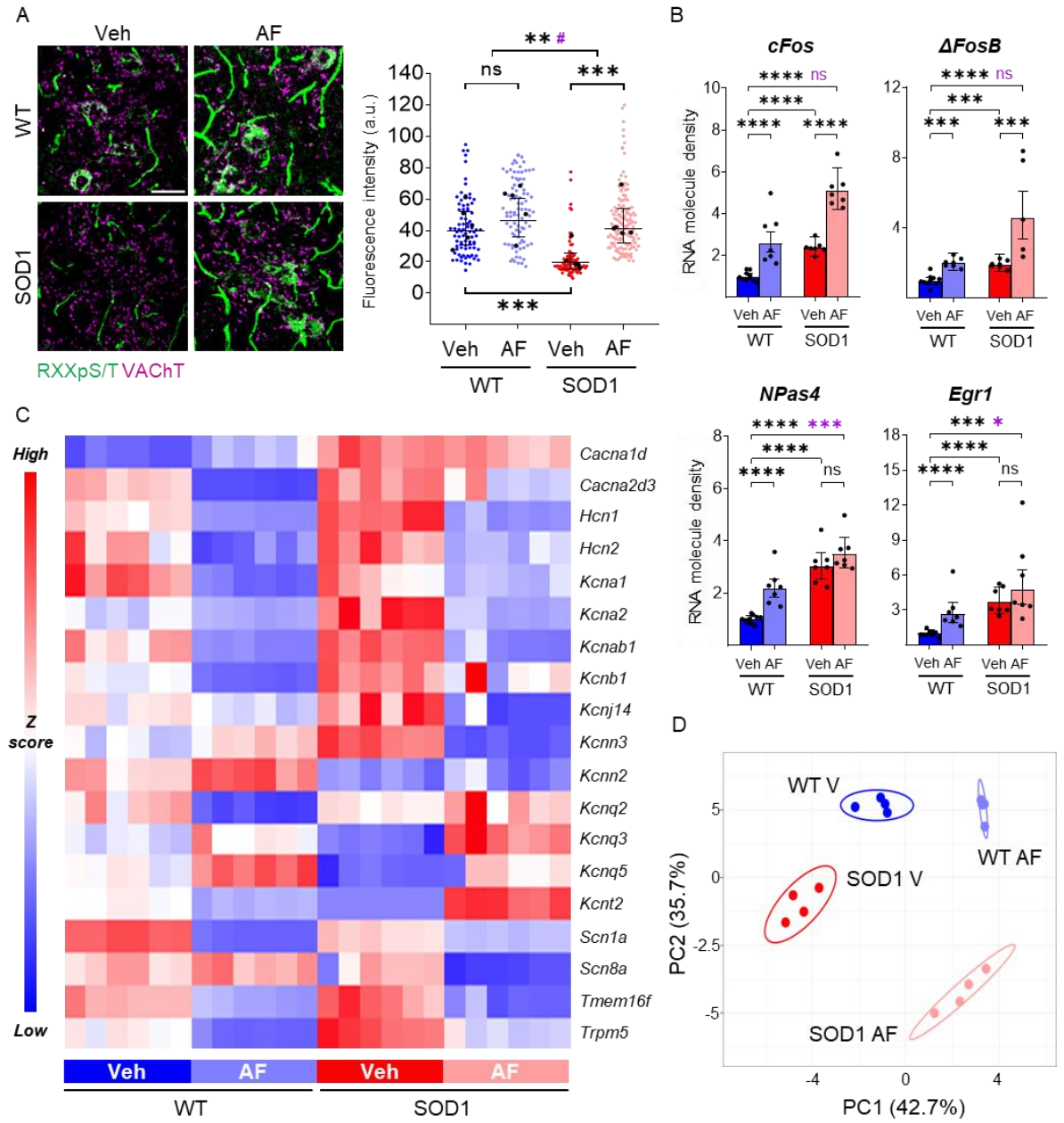


**Figure 2 | Acute pharmacological activation of β2/β3 receptors activates PKA signaling, induces Immediate Early Genes and modulates ion channel transcription. A)** Immunofluorescence reactivity for the consensus PKA-phosphorylated sequence RRxpS/T reveals increased immunoreactivity in the cytoplasm of MNs and in spinal vasculature upon β2/β3 stimulation in WT (strong trend, significant when the outlier animal is excluded) and SOD1 animals (Scale bar=50µm). In scatterplots, small dots correspond to individual MNs, large black dots to average per animal; mean and 95% confidence intervals are depicted. n= 5 per group. Treatment effects (black : treatment (above) or genotype (bottom) effect, magenta : interaction effect) **B)** Induction of IEG mRNA (*cFos*, *ΔFosB*, *NPas4*, *Egr1*) in MNs upon β2/β3 stimulation. Each dot represents an individual animal. Significance is indicated for treatment effects (black) or interaction effects (magenta). n=7-10 per group. **C)** Targeted ion-channel transcriptome in WT and SOD1 MNs reveals the broad downregulation of multiple channels upon β2/β3 stimulation. (downregulated genes*: blue*; upregulated genes: *red*). n = 6. **D)** PCA plot of IEG and ion channel gene transcription reveals the separation of the experimental group according to treatment and genotype. N = 4 mice per experimental group in which all genes were investigated.**p*<0.05, ***p*<0.01, ****p*<0.001, *****p*<0.0001.

3. *Acute adrenergic β2/β3 activation increases MN excitability in both WT and SOD1 mice.*

To investigate the impact of β2 and β3 agonists on intrinsic electrical properties of MNs, we relied on *in vivo* intracellular recordings carried out on anesthetized WT and SOD1 mice (see Methods). This approach allows us to investigate spinal MN in presymptomatic SOD1 mice at P45-P59, i.e. before the first denervations (Delestree *et al*., 2014, Martinez-Silva *et al*., 2018). In each experiment, we first recorded a sample of hindlimb MNs (between 1 and 7), then we i.v.-delivered the adrenergic β2/β3 agonists (cocktail of Formoterol and Amibegron; see Methods) before recording a new sample of MNs (between 1 and 9) in the next 3 hours following the drug delivery.

A series of depolarizing or hyperpolarizing pulses of currents (Fig. 3A-B) and a triangular slow ramp of current (Fig. 4A-B) allowed us to investigate whether the treatment with adrenergic β2/β3 agonists modify the physiological parameters that determine MN excitability (resting membrane potential, input conductance, voltage threshold for firing, recruitment current, firing gain; all statistics are detailed on Supplemental Excel Table 1). We found that the treatment does not significantly change the resting membrane potential both in WT and SOD1 motoneurons (Fig. 4C), nor the input conductance measured on the response peak (Gin Peak) at the onset of current pulses (Fig. 3C). In response to long pulses, the peak is followed by a sag down to a plateau that is caused by an H-current (Fig. 3A) (Ito and Oshima 1965, Takahashi 1990, McLarnon 1995, Manuel et al., 2009). We then also measured the input conductance at the end of the plateau (Gin Plateau, Fig. 3A-B) and we computed a sag ratio (ratio between Gin plateau and Gin peak). The treatment significantly reduces Gin plateau (Fig. 3D) and the sag ratio across genotypes (WT and SOD1) (Fig. 3E) suggesting that H-current has decreased. An almost significant interaction effect in both Gin Plateau and sag ratio suggests differences in treatment efficacy between genotypes with a stronger effect in SOD1 mice. In the same line, the input conductance measured at the beginning of the slow ramp (Gin ramp, Fig. 4B) is differently affected by treatment between WT and SOD1 mice (Fig. 4D). The treatment causes a significant reduction of Gin ramp in SOD1 mice but not in WT mice. It then appears that β agonists decrease Gin plateau and Gin ramp in MNs from SOD1 mice, likely through an action on H-current. This effect might increase MN excitability during slow depolarizing events.

Another parameter that sets MN excitability is the voltage threshold at which spikes are fired (V threshold). More hyperpolarized the voltage threshold for spiking, higher is the probability to elicit firing. We found that treatment causes a significant hyperpolarization of the voltage threshold in WT mice, suggesting an increased excitability, but not in SOD1 mice (Fig. 4E). The difference between voltage threshold and RMP (Vthreshold - RMP) is indeed significantly smaller after treatment compared to before, across genotypes (Fig. 4F). However, while the treatment seems to have a stronger effect in WT than in SOD1 mice, the difference between the two genotypes was not significant for Vthreshold - RMP. The next important parameter for assessing excitability is the amount of current required to reach the firing threshold recruitment current. During slow ramps, the voltage trajectory to reach the firing threshold is not linear since an acceleration occurred below the threshold for firing (Fig. 4B, arrow). This is why the recruitment current is smaller than the theoretical recruitment current that would be required in the case of a linear voltage trajectory (Delestrée *et al*., 2014). We found that treatment has a slight effect on the recruitment current which is reduced across genotypes (WT and SOD1 mice) (Fig. 4J), contributing to the excitability increase.

Once the discharge is initiated, the MN starts to discharge in the mixed mode oscillations regime, in which small oscillations (arrows in Fig. 4G) are present between spikes, describing a subprimary range, before transitioning to a regime of firing with full blown spikes whose frequency increases linearly with the injected current, i.e. the primary range (Fig. 4G, and see Manuel *et al*., 2009). Another important criteria to assess MN excitability is the slope (frequency-current gain) of the primary firing range (Fig. 4H), with a higher frequency-current intensity gain (F-I gain) indicating that the MN is more excitable. Indeed, the strongest action of β2/β3 agonists was observed on the F-I gain that is very significantly increased in MNs from both WT (64% increase) and SOD1 mice (63% increase) (Fig. 4K). Then, we asked, whether a faster kinetics of AHP current might contribute to the increase of the F-I gain (Meunier and Borejsza 2005, Manuel et al., 2006). We systematically measured the half-relaxation decay time on the AHP that follows the first 3-5 averaged spikes in the subprimary range, a range where AHP fully relaxed before the next spike (See Methods; Fig. 4I). Interestingly, the treatment caused significant shortening of the AHP half decay time across genotypes (Fig. 4L). The faster AHP kinetics is likely contributing to the gain increase.

To sum up, an acute administration of β2/β3 agonists increases MN excitability mainly through an increase of the F-I gain in both WT and SOD1 mice. However, a decrease of Gin plateau or Gin ramp in MNs from SOD1 mice, and an hyperpolarization of voltage threshold for spiking in MNs from WT mice may also contribute to the excitability increase induced by β2/β3 agonists.

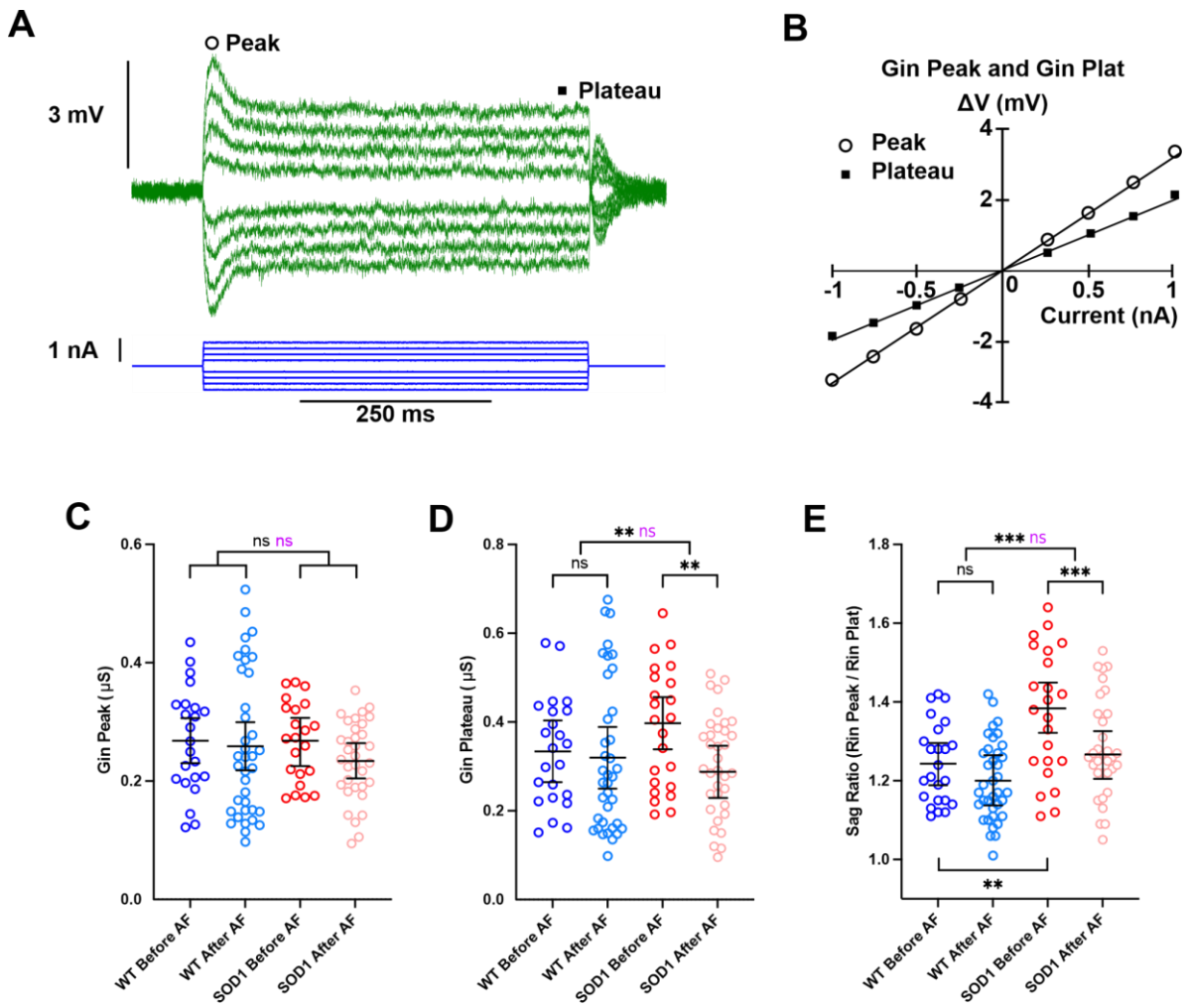


**Figure 3 | Acute delivery of adrenergic β2/β3 agonists decreases the plateau input conductance of motoneurons in SOD1 mice. A)** Average responses of a SOD1 MNs to a series of current pulses lasting 500ms and ranging from -1 to +1 nA. Notice the difference in the voltage response of the MNs: the sag formed by the voltage rapidly reaches a peak, before it stabilizes to a plateau value. **B)** Plot of the voltage-current response measured at the peak and plateau (as indicated in **A**) against the intensity of current. Effect of β2/β3 agonists on peak input conductance **(C)**, plateau input conductance **(D)**, and sag ratio (Gin plateau / Gin peak) **(E)** in MNs from WT and SOD1 mice. Significances on top bars are for treatment effects (black) and interaction effects (magenta). Post-hoc significances are shown for WT before AF *vs.* WT after AF (treatment effect in WT), SOD1 before AF *vs.* SOD1 after AF (treatment effect in SOD1) and for WT before AF *vs.* SOD1 before AF (genotype effect before treatment, bottom bar). Amibegron + Formoterol (AF). N = 6 WT mice and N = 11 SOD1 mice.*$p$<0.05, **$p$<0.01, ***$p$<0.001, ****$p$<0.0001, ns - non significant.

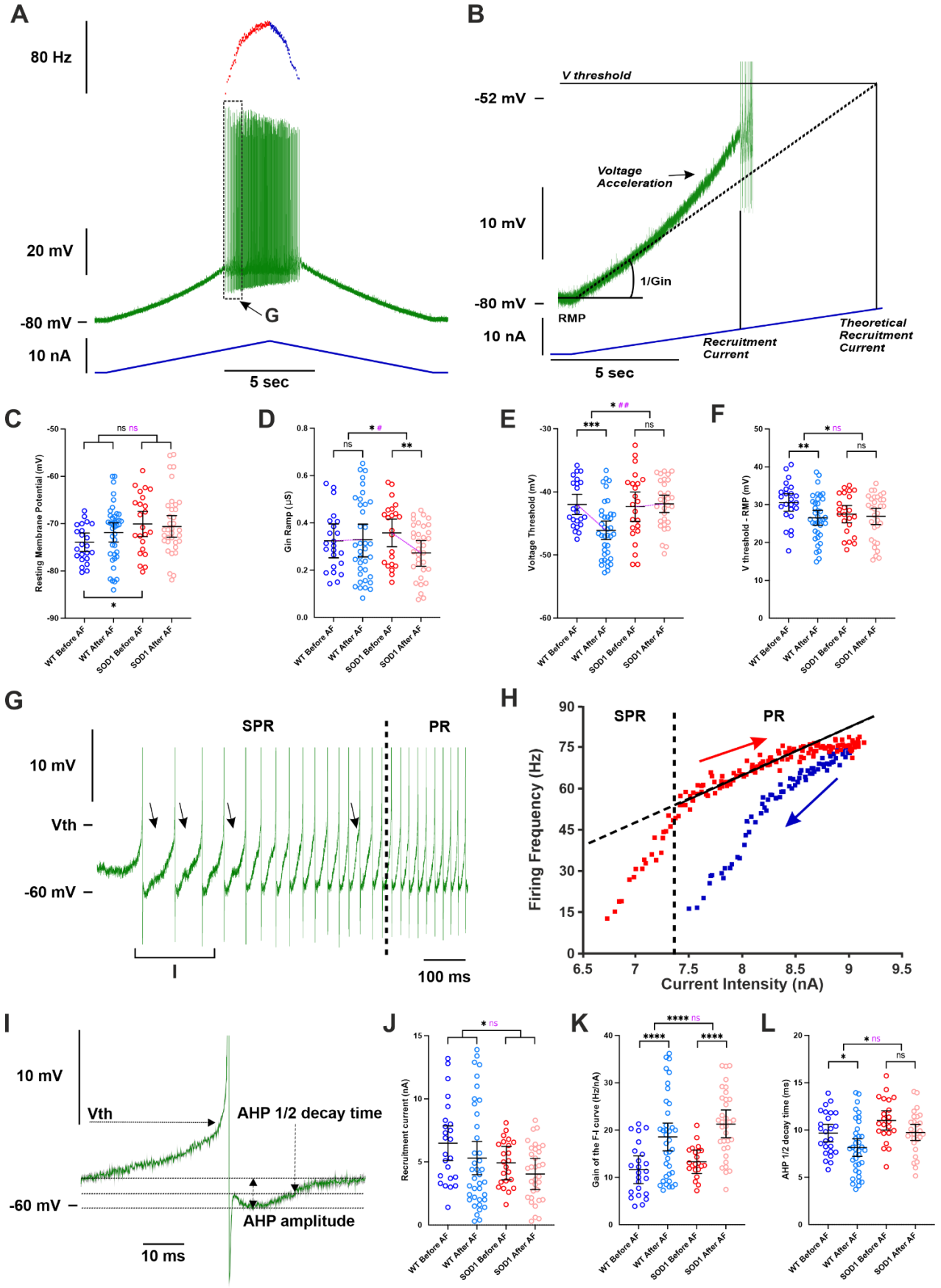


**Figure 4 | Acute delivery of adrenergic β2/β3 agonists increases the firing of motoneurons in WT and SOD1 mice. A)** Representative response of a SOD1 MNs to a slow ramp (1 nA.s$^{-1}$) of current. Ramp of current (blue bottom trace), voltage response (green middle trace) and instantaneous firing

frequency (top trace with ascending leg in red and descending leg in blue). **B)** Magnification of the ramp subthreshold voltage (green top trace) and current (blue bottom trace). The recruitment current is the minimum intensity to elicit a spike, while the theoretical recruitment current is the current intensity that would be needed to reach the voltage threshold (V threshold) if the MNs had no voltage acceleration and was a purely passive resistor (1/Gin). Effect of an acute delivery of Amibegron/Formoterol on resting membrane potential **(C)**, ramp input conductance **(D)**, voltage threshold for spiking **(E)**, voltage threshold - resting membrane potential **(F)**, recruitment current **(J)**, Gain of the F-I relationship **(K)**, AHP half-decay time **(L)** in MNs from WT and SOD1 mice. Magnification of the voltage trace from the region indicated in **A**. At the firing onset, oscillations (arrowheads) appear in the interspike intervals, which characterizes the subprimary range (SPR). When the injected current increases oscillations disappear, reducing the firing variability and increasing the firing frequency linearly, which characterizes the primary range (PR). **H)** Plot of the instantaneous firing frequency against the intensity of current for the ascending (red) and descending (blue) legs of the ramp shown in **A**. The F-I relationship displayed a clockwise hysteresis. Vertical dashed line indicates the transition between the SPR and the PR on the ascending leg. The gain of the F–I curve can be estimated by the slope of the linear regression (continuous line) in the PR. **I)** Average of the three first action potentials indicated in **G.** The AHP half-decay time is the time between AHP peak amplitude and where the AHP relaxed to half its amplitude. In all graphs, each point represents one MN and the mean ± 95% CI are shown. Significances on top bars are for treatment effects (black) or interaction effects (magenta). Post-hoc significances are shown for WT before AF *vs.* WT after AF (treatment effect in WT), SOD1 before AF *vs.* SOD1 after AF (treatment effect in SOD1) and for WT before AF *vs.* SOD1 before AF (genotype effect before treatment, bottom bar). Amibegron + Formoterol (AF). N = 6 WT mice and N = 11 SOD1 mice. *$p$<0.05, **$p$<0.01, ***$p$<0.001, ****$p$<0.0001, ns - non significant.

### 4. *Direct injection of cAMP analogue increases MN excitability from SOD1 mice.*

To confirm that the increase in the F-I gain of MNs upon β2/β3 adrenergic receptors activation was mediated by the activation of MN cAMP/PKA pathway (and not to alternative signaling, such as β-arrestin/ERK; Huang *et al*., 2018) and was not an off target effect (i.e. increase in heart rate), we directly activated the cAMP/PKA pathway by intracellular injection in MN of the cAMP analogue (cAMP-SP; Baczyk et al., 2020). We first recorded, before the injection, the responses of the MNs to a slow ramp of current and to long pulses (in order to determine the peak and the plateau input conductances). Then, we electrophoretically injected cAMP-SP through the intracellular microelectrode (normalized electrical load 2600 ± 600 nA.sec/µS, see Methods). We then recorded again the MN responses to slow ramps of currents and long pulses during at least 10 minutes. The whole procedure required that the MN recording did not deteriorate (see Methods) for at least 30 minutes, a condition that limited the number of successful experiments.

We have been able to follow the effect of cAMP-SP in 7 MNs from SOD1 mice (Fig. 5, statistics in Supplemental Excel Table 1). cAMP-SP significantly hyperpolarized the resting membrane potential (Fig 5C), and it slightly decreased the input conductance during the ramp (Gin Ramp, Fig 5D) (but it had no effect on the peak input conductance, plateau input conductance and sag ratio during long pulses). cAMP-SP also hyperpolarized the voltage threshold for spiking (Fig. 5E) but it did not

significantly modify Vthreshold-RMP (Fig. 5F), nor the recruitment current (Fig. 5G). However cAMP-SP significantly increased the F-I gain (average increase 32%, Fig. 5H) and, consequently, the maximal firing frequency measured at the end of the ramps (ramp velocity and amplitude were kept constant before and after cAMP-SP injection for each individual motoneuron) (Fig. 5I). In addition cAMP-SP shortened the AHP half decay time as acute β2/β3 agonists did (Fig. 5J). Altogether, many actions elicited in MNs by a direct activation of the PKA pathway (decrease of Gin Ramp, hyperpolarization of the voltage threshold, increase of the F-I gain, faster AHP kinetics) are the same as those produced by an acute i.v. delivery of β2/β3 agonists. These results strongly suggest that most of the β2/β3 agonists effects are caused by the activation of the cAMP/PKA pathway in MNs.

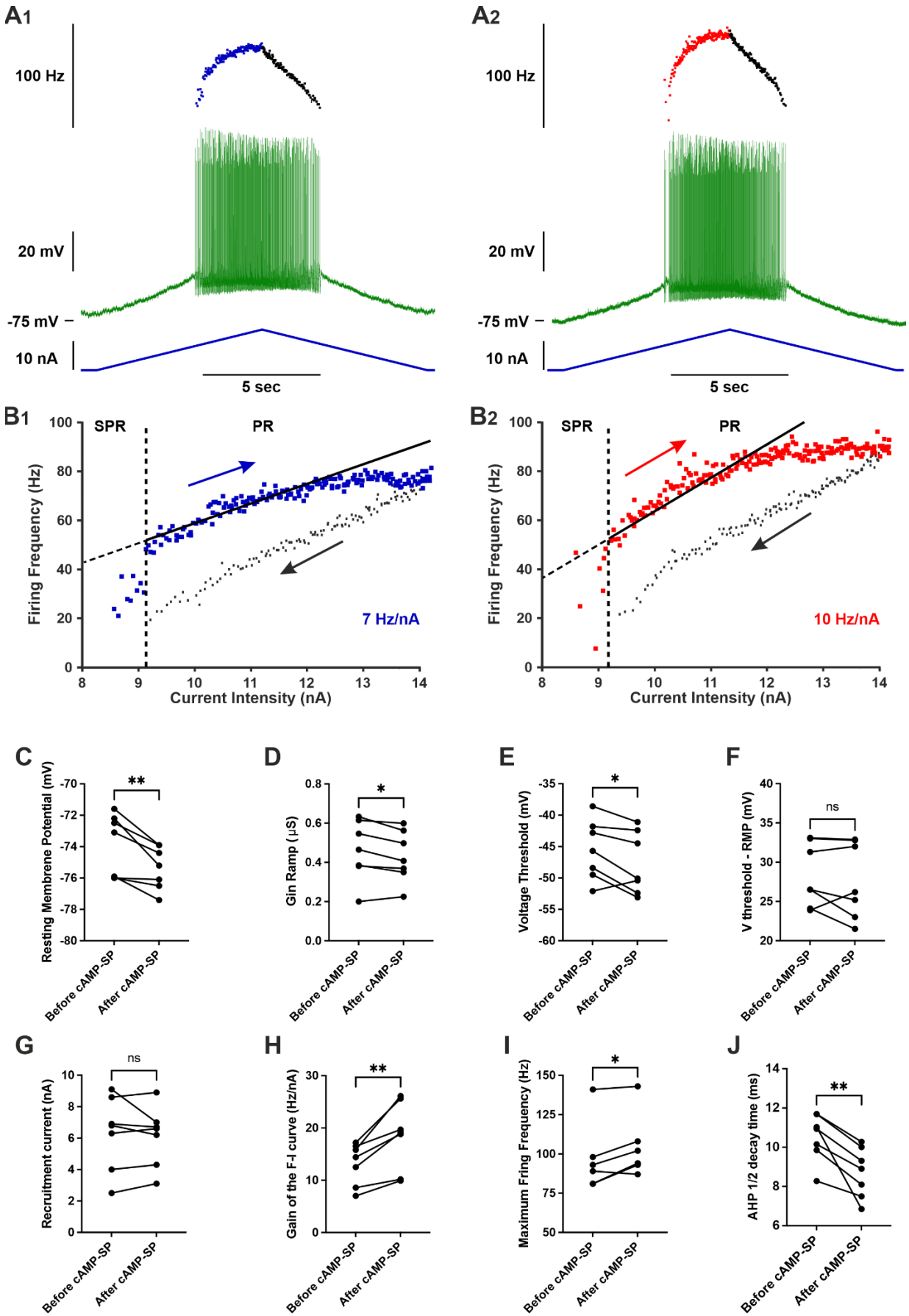


**Figure 5 | Activation of cAMP/PKA pathway increases the firing of motoneurons in SOD1 mice.** **A)** Representative response of a SOD1 MNs to a slow ramp (2nA.s-1) of current, before (**A₁**) and 12

minutes after (**$A_2$**) the iontophoretic injection of cAMP-SP in the same MNs. The ramp of current (blue bottom trace), voltage response (green middle trace) and instantaneous firing frequency (top trace with ascending leg in blue for **$A_1$** or red for **$A_2$**, and descending leg in black for both **$A_1$** and **$A_2$**. **B)** Plot of the instantaneous firing frequency against the intensity of current for the ascending (blue for **$B_1$** or red for **$B_2$**) and descending legs (black for both **$B_1$** and **$B_2$**) of the ramps shown in **A**. The F-I relationships displayed a clockwise hysteresis. Vertical dashed line indicates the transition between the SPR and the PR on the ascending branch. The gain of the F–I relationship can be estimated by the slope of the linear regression (continuous line) in the PR. **C-J)** Comparison of electrophysiological properties extracted from the slow ramp of current before and after injection of cAMP-SP. Before values are measured just before the injection; After values are averages of the recordings repeated after the iontophoretic injection of cAMP-SP; n=7 MNs recorded in N=7 SOD1 mice. **C)** Resting membrane potential. **D)** Ramp input conductance. **E)** Voltage threshold for spiking. **F)** Voltage threshold - resting membrane potential. **G)** Recruitment current. **H)** Gain of the F-I curve. **I)** Maximum firing frequency reached at the end of the ascending ramp (the velocity and amplitude were the same for all ramps in each MNs). **J)** AHP half-decay time. In all graphs, each linked two points represent one MN. Before vs. after values were compared using a paired t-test except for maximum firing frequency where a Wilcoxon paired test was used. *$p$<0.05;**$p$<0.01; ns - non significant.

### 5. *Prolonged β2/β3 adrenergic agonists downregulate PKA-coupled GPCRs in MNs*

In order to establish the therapeutic potential of protracted β2/β3 activation in MNs, we explored the effect on receptor expression either of chronic cAMP/PKA activation or of chronic β2/β3 stimulation. First, we used DREADD-Gs to stimulate cAMP/PKA in MNs (Fig. 6A-C); DREADD expression was obtained by intraspinal injection of AAV9 in SOD1/Chat-Cre double-transgenic mice (to restrict the expression to MNs; Baczyk *et al*., 2020). Upon administration of the cognate agonist (Clozapine-N-Oxide, 10 days), we observed a substantial downregulation of *Adrb1* in MNs (by SM-ISH; Fig.6A, 6C) but not of the PKA-coupled *Drd5* (Fig. 6B-C). On the other hand, 10-days administration of β2/β3 agonists resulted in the downregulation of *Adrb1*, *Adrb2* and *3* as well as of *Drd5* receptors (Fig. 6D), suggesting a potential loss of efficacy due to MN desensitization. In fact, assessment of β2/β3 agonists' impact on disease markers revealed no effect upon 10 days treatment on misfolded SOD1 burden (Fig. 6E).

We then performed electrophysiological experiments to investigate the effects of the prolonged treatment. Surprisingly we found that most of the effects of β2/β3 agonists disappeared upon chronic administration (Fig. 7, all statistics in Supplemental Excel Table 1). Gin peak (Fig. 7G), Gin plateau (Fig. 7H), sag ratio (Fig. 7I) and Gin ramp (Fig. 7D) were not affected anymore by the drug chronic delivery compared with vehicle. Vthreshold was not affected as well (Fig. 7B) but the drug has a small but significant effect on Vthreshold-RMP across genotype (Fig. 7C). However, this effect is due to a slight hyperpolarization of RMP (Fig. 7A). The recruitment current did not

significantly change either upon chronic drug delivery (Fig. 7E). More spectacularly, even the F-I gain, that was the most affected in acute conditions, did not change upon chronic conditions (Fig. 7F). Importantly, to ensure the reproducibility of these findings, we repeated the *in vivo* intracellular recordings in a second independent cohort in a different laboratory. Actually, the main findings were replicated : a single delivery of β2/β3 agonists increased the F-I gain but this effect is lost after a ten days administration (Supplemental Fig. 2D and 2H). It then looks like that the mRNA downregulation of *Adrb2* and *Adrb3* receptors during prolonged administration of β2/β3 agonists contribute to preventing the drug from increasing the MN excitability.

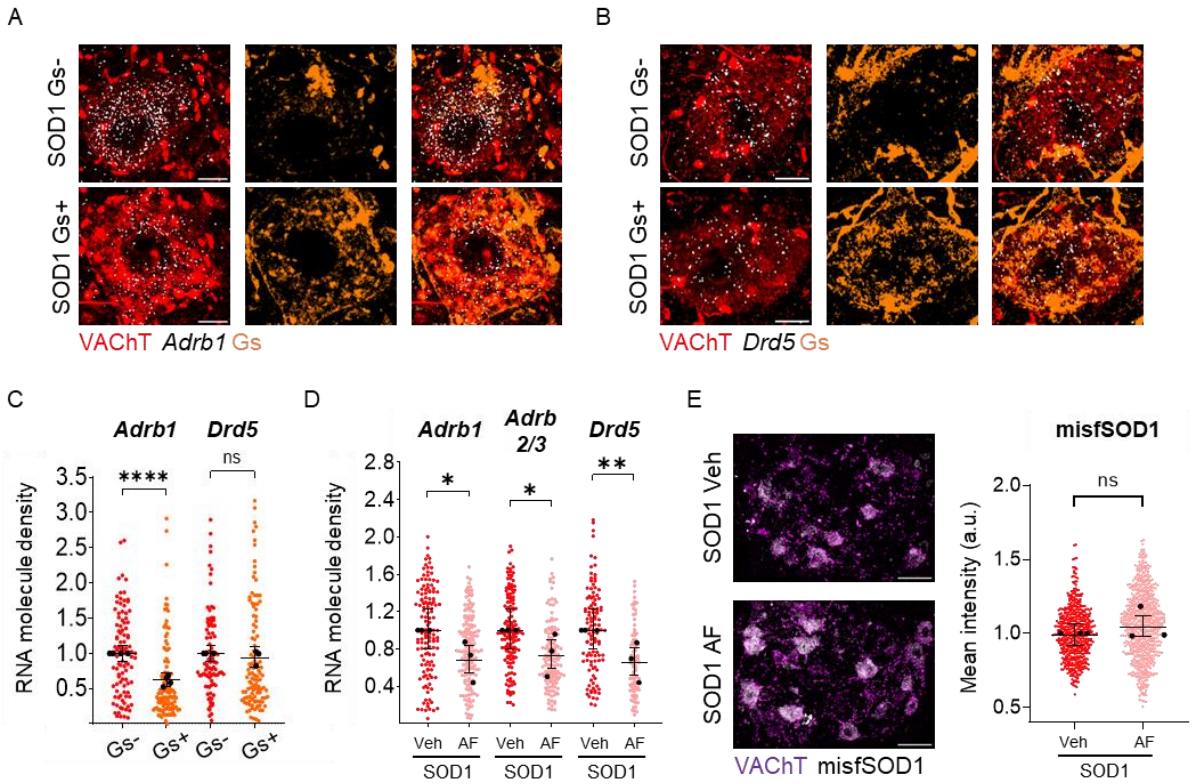


**Figure 6 | Chronic PKA engagement downregulates PKA-coupled receptors in MNs and does not result in amelioration of disease burden. A-C)** DREADD(Gs)-mediated chronic chemogenetic activation of PKA pathway in p45 SOD1 MNs results in the downregulation of *Adrb1* and *Drd5* mRNA. n = 4 mice for *Adrb1* ISH; n = 3 mice for *Drd5* ISH. Scale bar=10µm **D)** Expression of *Adrb1*, *Adrb2/3* and *Drd5*, revealed by single-molecule in situ hybridization, is downregulated by 10 days of β2/β3 agonists administration. n = 3. **E)** Immunofluorescence intensity (arbitrary units) of misfolded SOD1 immunostaining in MNs is not modified by 10 days β2/β3 agonists administration. *$p$<0.05, **$p$<0.01, ***$p$<0.001, ****$p$<0.0001, ns - non significant. Small dots correspond to individual MNs, whereas large dots indicate individual animal means; 95% confidence intervals are indicated.

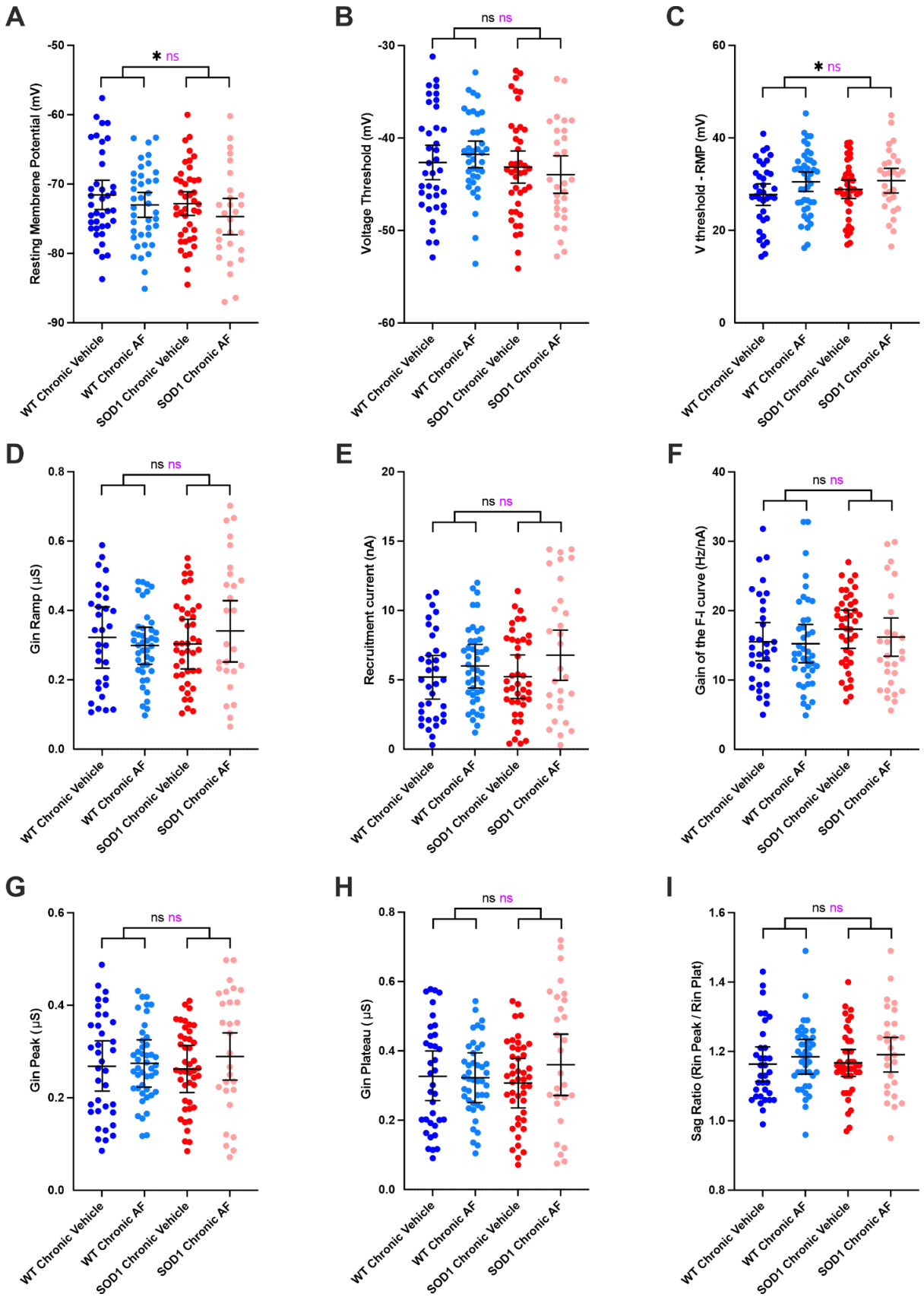


**Figure 7 | Prolonged delivery of adrenergic β2/β3 agonists does not increase the firing of motoneurons. A-F)** Electrophysiological properties were obtained from slow ramps of current, as in Figure 3. Effect of the treatment on resting membrane potential **(A)**, voltage threshold for spiking **(B)**, Voltage threshold - resting membrane potential **(C)**, ramp input conductance **(D)**, recruitment current **(E)**, gain of the F-I relationship **(F),** in MNs from WT and SOD1 mice. **G-I)** Electrophysiological properties

were obtained from series of current pulses lasting 500ms, as in Figure 3. Effect of the chronic treatment on peak input conductance **(G)**, plateau input conductance **(H)**, sag ratio (Gin plateau / Gin peak) **(I)** in MNs from WT and SOD1 mice. In all graphs, each point represents one MN and the mean ± 95% CI are shown. Significances on top bars are for treatment effects (black) and interaction effects (magenta). Post-hoc significances are shown for WT Chronic Vehicle *vs.* WT Chronic AF (treatment effect in WT), SOD1 Chronic Vehicle *vs.* SOD1 Chronic AF (treatment effect in SOD1) and for WT Chronic Vehicle *vs.* SOD1 Chronic Vehicle (genotype effect before treatment). N =11 WT mice and N = 9 SOD1 mice. *$p$<0.05, **$p$<0.01, ***$p$<0.001, ****$p$<0.0001, ns - non significant.

## Discussion

In the present paper, we demonstrate that the PKA-coupled receptorome of MNs, which includes no less than 30 receptors (whose physiological role remains to be explored in most cases), is substantially perturbed in ALS with the notable exception of β2 and β3 adrenergic receptors. We provide convergent evidence for a previously unappreciated role of β2 and β3 adrenergic receptors in the enhancement of MN excitability and firing, reflected in a distinct transcriptional response including the upregulation of IEGs as well as a dysregulation of ion channels genes both in WT and ALS MNs. However, the translational potential of β2 and β3 adrenergic agonists is limited by the homeostatic downregulation of their receptors (and of other PKA receptors) upon chronic administration, resulting in the loss of their neuromodulatory actions.

### An overlooked β-adrenergic modulation of spinal MN excitability

Noradrenergic (NA) descending fibers originating from the locus coeruleus and subcoeruleus are long known to innervate the spinal cord, where they were shown to play a role in initiating the locomotion (Jordan *et al*., 2007). Noradrenaline differentially modulates the activity of spinal interneurons involved in locomotion (Bras *et al*., 1990; Hammar *et al*., 2004). Descending noradrenergic fibers also directly contact spinal MNs. Each spinal MN was found to receive more than one thousands of NA contacts widely distributed throughout the dendritic arborization (Montague *et al*., 2013; Maratta *et al*., 2015). While noradrenergic neuromodulation of MN excitability through α-adrenergic receptors has been documented, neuromodulation through β-adrenergic receptors has received little attention so far. Actually, it was initially reported that MNs are endowed with α-adrenergic receptors but are deprived of β-adrenergic receptors (Nicholas *et al*., 1996). Many works reported multiple effects of noradrenaline on MN excitability (membrane depolarization, increased input resistance, hyperpolarization of the voltage threshold for spiking, reduction of AHP amplitude, increase of the F-I

gain…). These effects, may differ from one motor pool to another depending on its location in the brainstem or the spinal cord, but they were most of the time ascribed to α1 adrenergic receptors, sometime to α-2 receptors, but never to β-receptors (reviewed in Rekling *et al*., 2000). However a more recent investigation demonstrated the presence of β1 adrenergic receptors in lumbar MNs of neonate rats and showed that their pharmacological activation decreased the F-I gain (Tartas *et al*., 2010). To our knowledge, the present study is the only one that investigated the modulation of MN excitability by β2/β3-receptors. We demonstrated that FDA-approved β2/β3 adrenergic receptors agonists increase the excitability of MNs both in WT and in presymptomatic SOD1 adult mice, primarily through an increase of the F-I gain and, secondary, through a decrease of the stationary input conductance (Gin ramp, Gin plateau) in SOD1 mice and an hyperpolarization of the voltage threshold for spiking in WT mice.

**Neuromodulation of mAHP through β2/β3 adrenergic receptors**

It was established that the medium afterhyperpolarization (mAHP), which follows each action potential is a potent controller of the MN firing, in particular of the gain of the F-I relationship in primary range (Kernell 1999, Manuel *et al*., 2006). Indeed, in simple MN models, the F-I gain in primary range depends on the inverse of the product between AHP conductance, AHP decay time and AHP driving force (Meunier and Borejsza 2005, Manuel *et al*., 2006). The smaller and faster is the mAHP conductance, the higher is the F-I gain in the primary range. The AHP conductance is very difficult to measure (Manuel *et al*., 2005). However, we found here that β2/β3 adrenergic receptors agonists shortened the AHP half decay time indicating a faster kinetics of the mAHP conductance that accounts for, at least partly, the increase of the F-I gain. Furthermore, β2/β3 agonists reduce the voltage threshold for spiking in MNs from WT mice decreasing the AHP driving force that contributes to increase the F-I gain in these MNs. A secondary determinant of the frequency-current gain is the plateau input conductance (Meunier and Borejsza 2005) that was found to be reduced by β2/β3 agonists in MNs from SOD1 mice. In total the reduced AHP half decay time, voltage threshold for spiking and Gin plateau may all contribute to the increased frequency-current gain.

The mAHP current in rodent MNs is mainly caused by the SK2 and SK3 calcium-dependent potassium channels, which were found to cluster on soma and proximal

dendrites of α-MNs at the level of C-boutons (Deardoff *et al*., 2013). Indeed, blockade of SK channels with apamin increases the gain of the F-I relationship in spinal MNs (Zhang and Krnjevic 1987). How do β2/β3 receptors act on the SK channels? Indeed, SK channels display constitutive trafficking, and PKA activation was shown to decrease the surface expression of SK channels through three phosphorylation sites ($Ser^{568}$, $Ser^{569}$ and $Ser^{570}$ at the carboxyl-terminal region) (Ren *et al*., 2006). In the present work, we showed that an intracellular injection of cAMP-SP (a cAMP agonist) also increases the F-I gain relationship, similarly to the systemic delivery of β2/β3 agonists. Furthermore, we also showed that the pharmacological stimulation of the β2/β3 adrenergic Gs-coupled receptors effectively engages the cAMP/PKA pathway. We then speculate that the pharmacological stimulation of β2/β3 adrenergic receptors indirectly removes SK channels from the plasma membrane of MNs through the activation of the cAMP/PKA pathway. A similar scenario was previously demonstrated at excitatory synapses from lateral amygdala pyramidal neurons (Faber *et al*., 2008). This would result in a decrease of the SK conductance, entailing an increase of the F-I gain in the primary range, as observed in our experiments.

In addition to SK channels, voltage-dependent $K_V2.1$ channels were recently found to contribute in setting the F-I gain (Romer *et al*., 2019, Nascimento *et al*., 2020). Many $K_V2.1$ channels are located at C-boutons, where they are in a highly-phosphorylated form, and are clusterized and intermingled with SK clusters (Deardorff *et al*., 2021). At the opposite of SK channels, blocking $K_V2.1$ channels with tarantula toxin stromatoxin (STX) decreases the F-I gain in lumbar MNs (Rommer *et al*., 2019). However, $K_V2.1$ phosphorylation is mainly caused by the cyclin-dependent kinase 5 that is not directly linked to the cAMP/PKA pathway (Cerda and Trimmer, 2011).

**Adrenergic vs cholinergic modulation of SK channels**

The mechanism for β2/β3-adrenergic neuromodulation of SK channels is most likely different from the cholinergic neuromodulation of SK channels. At C-boutons, acetylcholine acts through m2 receptors, which are coupled to Gi/Go intracellular pathways. How m2 receptor activation reduces the SK current remains unclear (Miles *et al*., 2007). However, It was suggested that m2 activation could inhibit voltage-gated calcium channels, thereby reducing the activation of the calcium-dependent SK channels (Deardorff *et al*., 2013). Whatever the case, a β2/β3-adrenergic modulation of these channels may occur if β2/β3 receptors are located in vicinity to SK channels.

However this could not be tested since we did not find specific antibodies against β2/β3 receptors.

**Chronic β-adrenergic stimulation results in homeostatic mechanisms that cancel physiological effects.**

Prolonged β2/β3 agonists treatment of either WT or SOD1 animals results, in our experiments, in the loss of their neuromodulatory effects on MN electrophysiological properties. This homeostatic response may be caused by several mechanisms at transcriptional, post-transcriptional and post-translational levels. 1) We show that the β2/β3 mRNA is downregulated upon chronic pharmacological stimulation of the β2/β3 receptors establishing a negative feedback loop. Notably, heterologous downregulation of other Gs-coupled GPCRs is observed upon β2/β3 agonists treatment (or chemogenetic stimulation of Gs signaling). Our findings are in agreement with the downregulation of adrenergic receptors mRNA in multiple organs upon chronic adrenergic stimulation (Mak *et al*., 1995; Lefkowitz *et al*., 2000; Milano *et al*., 2018) through mechanisms involving transcriptional regulation and mRNA stability (Danner *et al*., 1998), as well as with extensive heteronomous downregulation of Gs-coupled GPCRs. 2) A single injection of β2/β3 agonists substantially dysregulates the channelome with a pattern compatible with reduced motoneuron excitability. Indeed, while β2/β3 agonists increase the gain, *Kcnn2* (SK2) and *Kcnn3* (SK3) are upregulated in WT motoneurons (pointing toward reduced excitability, although not in the SOD1 ones), and *Kcnb1* ($K_v$2.1) is downregulated in both WT and SOD1. In the same line, while β2/β3 agonists hyperpolarize the voltage threshold for spiking in WT, *scn1a* (Nav1.1, sodium current) is strongly downregulated in WT and moderately in SOD1, again pointing toward reduced excitability, and *Kcnq3* (Kv7.3, M-current) is upregulated in both WT and SOD1 motoneurons (however *Kcnq2* is downregulated in WT). We notice that β2/β3 agonists also downregulate *Tmem16f* and *Trpm5* in WT and SOD1 that were shown to decrease the rheobase (Soulard *et al*., 2020) or to facilitate bistable behavior (Bos *et al*., 2021), respectively. Even if these transcriptional changes may only partially translate into protein-level changes within the time frame of the acute experiments, they would be relevant in the context of the ten-days pharmacological stimulation (chronic condition). 3) Post-translational mechanisms may also contribute to stabilizing β-adrenergic signaling against persistent stimulation. Upon activation, phosphorylation of the cytoplasmic tail of adrenergic receptors results in their interaction with β-arrestin adaptors that mediate their endosomal internalization

and thereby signal desensitization (Hausdorff *et al*., 1991; Tran *et al*., 2004; Wachter and Gilbert, 2012) in a timeframe of minutes to hours. Moreover, persistent stimulation leads to the phosphorylation of the receptors by β-adrenergic receptor kinases (BARKs) triggering a switch in the affinity from Gs to Gi and the reversal of the Adenylyl Cyclase activation (Wang *et al*., 2017). These post-translational homeostatic mechanisms extend to other convergent receptors through heterologous desensitization mechanisms involving PKA phosphorylation (Benovic *et al*., 1985; Gainetdinov *et al*., 2004). To sum up, our findings show that, both healthy and ALS MNs display substantial homeostatic loops regulating PKA signaling and excitability responses to GPCR stimulation.

**Conclusions**

Our findings demonstrate that MNs are responsive to neuromodulatory signals not only from α- but also from β-adrenergic receptors, hinting at an integration of these two distinct adrenergic signaling cascades with each other and possibly with other neuromodulators. We demonstrate that homeostatic processes, at receptor and ion-channel levels, are set in motion by β-adrenergic stimulation aimed at restoring an excitability set-point. These homeostatic loops are active both in normal and disease conditions and should be factored in when therapeutic interventions aimed at these and similar receptors are explored.

## Acknowledgments

The authors acknowledge the animal facility of BioMedTech *Facilities* at Université Paris Cité (INSERM US36 / CNRS UAR2009) for its support and expertise. We thank the Thierry Latran Foundation (“TRiALS” project), the National Institutes of Health, National Institute of Neurological Disorders and Stroke (R01NS110953), the join Deutsche Forschungsgemeinschaft/Agence Nationale de la Recherche “SynaptALS” project (ANR-20-CE92-0029-01/ DFG 446067541), the Deutsche Forschungsgemeinschaft (no. 443642953) and Polish National Science Centre (OPUS 2019/35/B/NZ4/02058) for their financial support.

## Authors contributions

Conceptualization, M.B., F.R., D.Z., Methodology, S.A., M.B., G.C., S.D., F.R., Software, S.A., S.D., Formal Analysis, S.D., Investigation, S.A, M.B., A.T., H.Z., G.C.,

K.G., S.S.K., Data Curation, G.C., S.D., Writing-original draft, S.A., M.B., G.C., S.D., F.R., D.Z., Writing - Review & Editing, A.L., S.A., M.B., G.C., S.D., F.R., D.Z., Visualization, S.A., G.C., Supervision, M.B., F.R., D.Z., Funding Acquisition, A.L., M.B., F.R., D.Z.

## Methods

### Animals

All experiments were performed on the transgenic mouse line B6SJL-Tg(SOD1*G93A) 1Gur/J pursued via The Jackson Laboratory (#002726, Gurney *et al*., 1994). SOD1*G93A hemizygotes (here referred to as SOD1) develop a phenotype resembling human ALS as a consequence of the high number of transgene copies. Only males were used in Ulm (transcriptomics experiments), given the well-known sexual dimorphism in ALS (Trojsi *et al*., 2020); in accordance with literature characterizing disease staging in this mouse strain (Gurney *et al*., 1994; Saxena *et al*., 2013; Ouali Alami *et al*., 2018; Bączyk *et al*., 2020), animals aged P40-P45 were deemed presymptomatic and P110 fully symptomatic. Animal experiments from Ulm were conducted according to institutional guidelines (Tierforschungszentrum, Universität Ulm, Germany) under the approval of the Regierungspräsidium Tübingen with license nr. 1390 (untreated) and 1440 (drug-treated animals).

Animal experiments from Paris were approved by the Paris Descartes University ethics committee (CEEA34) and authorized by the french ministry for higher education and research (authorization number APAFIS#16338-2018052100307589). Animal experiments from Poznań were approved by the local ethical committee (16/2021). For electrophysiological experiments in Paris and in Poznań, both male and female mice were recorded between the ages of P45-P59.

Mice were grouped ≤5 with access to food and water *ad libitum* and housed in M2 long cages in an open shelving system (Ulm, Poznań) or disposable and ventilated cages (Paris) under a 12h/12h light/dark cycle with 40÷60% relative humidity. Upon routine tests assessing motor impairment, individuals reaching end-stage (on average >P110-P120) were euthanized complying with the aforementioned directives. In Paris, mSOD1 mice were euthanized no later than P90.

For electrophysiological experiments B6SJL-Tg(SOD1*G93A)1Gur/J males were crossed with B6SJL/J females, and offspring carriers of the mutated SOD1 gene were selected for experimental groups (SOD1), with non-transgenic littermates serving as wild type (WT) control animals. For chemogenetics experiments (Regierungspräsidium Tübingen, license nr. 1404), females from the B6;129S6-Chat tm2(cre)Lowl /J line (The Jackson Laboratory, stock #006410; Rossi *et al*., 2011) were

crossed with SOD1 males; only F1 SOD1;Chat-Cre males were used for intraspinal injections of AAV9 viruses enabling Cre-dependent expression of the Gs-DREADD construct in ChAT+ cells (viruses were produced as in Commisso et al., 2018).

**Surgical procedures for electrophysiological experiments**

In Paris and Poznan, electrophysiological experiments were carried out with the same protocol. Fifteen minutes before anesthesia, atropine (0.20 mg/kg; Aguettant or Polfa) and methylprednisolone (0.05 mg; Solu-Medrol; Pfizer) were given subcutaneously to prevent salivation and edema, respectively. Anesthesia was induced with an i.p. injection of Fentanyl 0.025 mg/kg, Midazolam 7.5 mg/kgl and Medetomidine 0.5 mg/kg. The heart rate was monitored with an EKG, and the central temperature was kept around 37°C using an infrared heating lamp and an electric blanket. Then, the mouse was artificially ventilated with pure oxygen (SAR-1000 ventilator; CWE) through a cannula inserted in the trachea. The ventilator settings were adjusted to maintain the end-tidal CO2 level at ∼4% (Micro-Capstar; CWE). Two catheters were introduced in the external jugular veins. The first one was used to deliver supplemental doses of anesthesia whenever necessary (usually every 20–30 min) by i.v. injection (10% of the dose used for anesthesia induction). The adequacy of anesthesia was assessed by lack of noxious reflexes and stability of the heart rate (usually 400–500 bpm) and end-tidal PCO2. The other catheter was used to slowly inject (50 µl/h) a 4% glucose solution containing NaHCO3 (1%) and gelatin (15%; Voluven; Fresenius Kabi or Tetraspan; Braun) to maintain the physiological parameters and to inject the tested treatment. The sciatic nerve was dissected and mounted on a bipolar electrode for stimulation. The vertebral column was immobilized with two pairs of horizontal bars (Cunningham Spinal Adaptor; Stoelting) applied on the Th12 and L2 vertebral bodies, and the L3–L4 spinal segments were exposed by a laminectomy at the Th13–L1 level. The exposed tissues from the hindlimb and spinal cord were covered with pools of mineral oil. When the surgery was completed, the animal was paralyzed with vecuronium or pancuronium with a bolus of 0.5mg/kg as needed. Additional doses of anesthetic were then provided at the same frequency as before the paralysis, and adequacy of anesthesia was assessed by stability of the heart rate and PCO2. At the end of the experiment, animals were euthanized with a lethal i.p. injection of pentobarbital (Exagon or Morbital; 80mg).

**Stimulation and intracellular recordings**

Intracellular recordings of MNs were performed with micropipettes (tip diameter, 1.0–1.5 μm) filled with 2 M K-acetate (resistance ∼25 MΩ). Recordings were made using an Axoclamp 2B (Paris) or Axoclamp 900A (Poznań) amplifier (Molecular Devices) connected to a Power1401 interface (sampling rate 20 kHz) and using Spike2 software (CED). After impalement, identification of MNs relied on the observation of antidromic action potentials in response to the electrical stimulation of the sciatic nerve. All MNs retained for analysis had a resting membrane potential more hyperpolarized than −50 mV and an overshooting action potential >65 mV. For more details on the analysis, see Manuel *et al*. (2009).

Briefly, the input conductance was determined from the I-V relationship, which was plotted from the peak (Gin peak) and plateau (Gin plateau) responses to a series of small-amplitude square current pulses (−2 to +2 nA, 500 ms). The sag in the voltage responses at the peak and plateau indicates the presence of an Ih current (McLarnon, 1995), which was estimated by computing the “sag ratio” (Gin peak / Gin plateau). Discharge properties were investigated using slow triangular ramps of currents (0.5 - 2 nA/s). The discharge frequency-current relationship (F-I) was determined by plotting the instantaneous firing frequency against the current intensity. The input conductance was also determined from the early linear voltage response (<2 nA) to a slow ramp of current (Gin ramp). This allowed us to calculate the theoretical recruitment current, which is the current intensity that would be needed to reach the voltage threshold if the MN had no voltage acceleration and was a purely passive resistor. All recordings were performed in discontinuous current clamp mode (8 kHz). All care was taken to compensate for the microelectrode resistance and capacitance.

**PKA activation experiments**

The procedures for surgery, MN stimulation and recording were performed as described above. To measure the impact of PKA activation on MN intrinsic excitability, the recording microelectrode was filled with a mixture of 2 M K-acetate, and 4 mM cAMP analogue (S)-adenosine, cyclic 39,59- (hydrogenphosphorothioate) triethylammonium (cAMP-SP; Sigma). Upon penetration of a MN, series of square current pulses and slow ramp of currents were repeated in successive 3-5 min intervals for at least 15 min, until the properties of the MN stabilized. Then, the iontophoretic injection of cAMP-SP was performed through the microelectrode (500 ms pulses of −2 to −4 nA, repeated at 1 Hz, total normalized electrical load injected 2600 ± 600 nA.sec/µS. We adjusted the injected current to the MN input conductance (normalized electrical load) because we noticed that MNs with higher conductance needed more current injection to observe the same effects as in MNs with smaller conductance. Immediately after, the square current pulses and slow ramp of currents were repeated with the same parameters as before the activation of the cAMP/PKA pathway. Data were excluded when the resting membrane potential changed by more than ±5 mV or the bridge balance changed by more than ± 20%, to ensure that the changes in excitability are not due to an insufficient stability of the MN or the microelectrode.

**Surgical procedures for intraspinal AAV injections**

Intraspinal surgery and AAV injection procedures were performed as in Bączyk *et al*. (2020). In short, P18 to P21 mice first received a s.c. dose of buprenorphine (0.1mg/kg) and meloxicam (1mg/kg) and from then onwards they were kept anesthetized onto the stereotaxic frame via continuous administration of 2% isofluorane in $O_2$ at 0.8L/min $O_2$ flow rate. After making a small incision on the skin, the subcutaneous fascia was removed and the paraspinal muscles were gently pushed sideways and blunt dissected. The underlying spinal cord was exposed by conducting laminectomy on T12 and removing the vertebral bone flap. Using a Picospritzer microfluidic device, 1µL of a 1:1 mixture of virus suspension and 1% Fast Green dye in PBS++ was injected with a pulled glass capillary at the following stereotaxic coordinates: y=+0.25mm with respect to the dorsal artery; 0.4mm depth below the dorsal surface of the spinal cord. Before withdrawing it, the capillary was left

in place for 10 minutes to allow the viral suspension to diffuse locally and to avoid viral backflow. Over the next 3 days, mice were treated with meloxicam (daily, 1mg/kg) and buprenorphine (twice a day, 0.1mg/kg) and monitored for post-operative complications.

**Drug treatments**

The Adrb ligands selected for acute or chronic (10 days-long) intraperitoneal (i.p.) treatment were amibegron (A; Cayman Chemicals 11954), an Adrb3 agonist, and formoterol fumarate (F; LKT Laboratories F5868), an Adrb2 agonist. All drugs were diluted in a mixture of 5% dimethyl sulfoxide (DMSO) 5% Tween-80 5% polyethylenglycole-400 (Roth) in saline to achieve the designated daily dosage (AF, 10mg/kg A and 0.3mg/kg F). Intracardiac perfusions took place 3h after the latest injection.

For electrophysiological experiments, A and F stock solutions were separately diluted in DMSO (Sigma) and stored at -20°C until the day of the experiment. The day of the experiment, stock solutions were diluted in saline (B.Braun) and mixed together to obtain the desired dose (A: 3 mg/kg and F: 0.3 mg/kg). The AF cocktail was injected i.v. after at least one MN was recorded. Just after the injection of AF, an increased heart rate was clearly observable on the EKG and started to decrease after 3h. Because β-adrenergic receptors are expressed in the heart and are known to increase the heart rate (Lohse *et al*., 2003), we used the heart rate as an indicator of an ongoing activation of β-adrenergic receptors. Therefore, MNs were recorded and kept for analysis for up to 3h after the injection of AF.

For chemogenetics experiments, mice injected with Gs-DREADD-expressing AAV9 were administered the Gs-DREADD agonist clozapine N-oxide (CNO) between P35 and P45 i.p. route twice per day at 5mg/kg, with an 8h interval between consecutive treatments. Drugs were solubilized in DMSO and diluted in saline (2.5% DMSO in the final mixture). Intracardiac perfusions took place 3h after the last injection.

**Laser capture microdissection and RT-qPCR**

Mice received terminal anesthesia by i.p. administration of ketamine (100mg/kg; WDT) and xylazine (16mg/kg; Bayer) and were perfused with RNAse-free ice-cold PBS for 2

min at 7mL/min flow rate. The lumbar portion of the spinal cord was quickly dissected out, OCT embedded (Sakura) and stored at -80°C. 12µm-thick cryosections were converted onto RNAse-free polyethylene terephthalate membrane (PET) slides (Zeiss 415190-9051-000) after these had been coated with poly-L-Lysine (Sigma Aldrich).

Firstly, a fixation step was performed in -20°C-cold 70% ethanol in RNAse-free $H_2O$ (DEPC $ddH_2O$ : 1% diethylpyrocarbonate (Roth) in $ddH_2O$). Next, the slides were stained for 1 min in 4°C-cold 1% cresyl violet (WALDECK) in 50% ethanol-DEPC $ddH_2O$ and finally washed for 1 min in 4°C-cold 70% and then 100% ethanol-DEPC $ddH_2O$. 30 MNs per group were microdissected into 500µL adhesive caps (Zeiss) with a laser microdissection system (Palm MicroBeam, Zeiss). MNs were lysed by pipetting 21µl of a mixture comprising 30µl 10X RT buffer, 3µl RNAse OUT (Invitrogen™ SuperScript™ III Reverse Transcriptase kit, 11904018) and 0.3µl 1%NP-40 in $ddH_2O$ directly onto the adhesive cap. After vortexing upside-down for 30s and incubating for 20 min at 42°C, samples were frozen at -80°C overnight.

Reverse transcription and RNA digestion were carried out with the cDNA synthesis kit as per manufacturer's instructions. RNA content was determined via qPCR with a Roche LC480 cycler using 2µl cDNA. PCR cycles were set as follows: 2 min at 50°C, 10 min at 95°C (initial denaturation); 50 cycles comprising 15 s at 95°C (denaturation) and 1 min at 60°C for annealing and elongation. The relative quantification of the transcripts of interest relied on the ΔCt method upon normalization against *Gapdh* housekeeping gene; the sequences of the primers used in this study, designed with NCBI Primer designing tool (Primer-BLAST, Ye et al.,, 2012) are reported in Suppl. Table 1.

**Histology**

Terminally anesthetized P45 animals were perfused first with 50mL ice-cold PBS (prepared in house) and 50mL 4% paraformaldehyde (PFA; Sigma-Aldrich) in PBS at an approx. 7mL/min flow speed. Overnight fixation in 4% PFA in PBS preceded incubation in 30% sucrose (Roth) in PBS and OCT embedding. Samples were equilibrated overnight at -20°C before being sequentially cut into 15µm-thick sections.

*In situ* hybridization (ISH) experiments were carried out with the RNAscope Fluorescent multiplex reagent kit v1 (Advanced Cell Diagnostics, ACD; Wang *et al*., 2012) and the following ACD probes: Mmp9-C1 (315941), Adrb1-C3 (449761), Hrh3-C3 (428481), Adora2b-C3 (445281), Drd5-C3 (494411), Adrb2-C3 (449771), Adrb3-O1-C3 (502581), Chrm2-C2 (495311). The manufacturer protocol for fixed frozen tissue was followed with minor deviations (refer to Olde Heuvel et al., 2019 for detailed procedures).

Subsequently, sections were co-immunostained to identify α-MNs; to prevent ISH signal disruption, the slides were always incubated in a humid chamber and protected from light. In short, sections were washed twice in 1X Wash Buffer for 10 min at room temperature (RT), incubated for 1h at RT in blocking buffer (BB: 10% Bovine Serum Albumin 0.3% Triton™X-100 (Sigma-Aldrich) in 1X PBS) and finally with primary antibodies overnight at 4°C. In this manuscript primary antibodies (anti-VAChT, Synaptic Systems, 139105; anti-mCherry, NanoTag Biotechnologies, N0404-AT565) were pre-diluted 1:250 in BB. Three 30 min washes in 0.1% Triton™X-100 in 1X PBS (PBS-T) at RT preceded incubation with pre-diluted secondary antibodies (1:250 in BB) for 2h at RT. All secondary antibodies (Sigma, SAB4600468 used for co-immunostaining were applied at 1:250 dilution. For free-floating immunostaining experiments, sections were incubated in BB for 2h and with primary antibodies (anti-misfSOD1 1:1000, Médimabs MM-0070; anti-VAChT 1:500, Synaptic Systems, 139105; anti-phospho-PKA substrate 1:100, CST 9621) for 48h; secondary antibodies (Invitrogen, A21202; Biotium, 20171; Invitrogen, A32790) were applied at 1:500 dilution.

**Imaging**

All experiments comprising an ISH step were imaged using a confocal laser scanning microscope (Carl Zeiss LSM710) equipped with a Plan-Apochromat 63X oil objective (NA 1.40). Images were acquired with a 1024x1024 frame size at 12-*bit* depth (0.132µm/px resolution in *xy*; 0.57µm voxel depth) preferentially at the surface of the section where probe penetration was highest and thus consistent between groups. The same image acquisition settings were employed to image misfSOD1 accumulation and phospho-PKA epitopes, but with a 20X objective (NA 0.8). Only ventrolateral MNs were investigated in this study.

**Image processing and quantification**

Maximum intensity projections of confocal *z*-stacks and in general all downstream processing and image analysis steps were instead performed in *Fiji* (Schindelin *et al*., 2012). *ImageJ* custom macros enabled semi-automated identification, drawing and ID assignment of MN *somata* according to VAChT signal. Regions of interest (ROIs) were then extracted from ISH channels (upon a background subtraction step, *radius* 5) and their size was measured retaining information on the receptor probe, the experimental group and the MN ID in their name tag. A similar approach was adopted to measure cytoplasmic PKA phospho-epitopes and whole-cell misfSOD1 accumulation as mean fluorescence intensity per MN cross section area. ISH signal was quantified as spot density per $\mu m^2$ by means of custom Jython and *ImageJ* macro scripts exploiting the difference of Gaussian detector shipped with Trackmate plugin (Tinevez et al., 2017); peak size and intensity threshold were set upon visual inspection of the experimental group given the slight variability and efficiency of probe penetration in different batches.

**Data analysis and statistics**

All RT-qPCR data were first normalized against *Gapdh* mRNA levels and, subsequently, against the control group (WT group for the LCM-based GPCR screening; WT vehicle for acute drug treatment experiments; SOD1 vehicle for chronic administration experiments). To test whether MN mRNA expression differed between WT and SOD1 mice, a t-test for each gene was computed. For the P45 LCM-based data, heatmaps were generated with the *ggplot2* R package.

All ISH and misfSOD1 immunohistochemistry data were first normalized against the control group for a meaningful comparison of the experimental sets; a quality-control step was further included to determine MN cross-section areas and assess whether the sampling was uniform or otherwise introducing unintended bias. Upon data inspection of P45 receptorome scatterplots (*Mmp9* vs receptor), for all screenings a threshold of 0.3 spots per $\mu m^2$ was chosen in order to subdivide MN into *Mmp9*+ and *Mmp9*- categories. Data from *Chrm2* (both timepoints), *Adrb2 and Adrb3* were handled with the *tidyverse* R package.

For GPCR ISH screening, to test whether MN mRNA expression differed between WT and SOD1 mice and whether this effect was different between *Mmp9*- and *Mmp9*+ MNs, a generalized linear mixed model was calculated for each gene. Fixed effects for genotype (WT or SOD1) and motoneuron type (*Mmp9*- or *Mmp9*+), their interaction effect, a random per-animal offset, and a full-factorial dispersion model were included. A gaussian error distribution with an identity-link was used, except for *Chrm2*, *Drd4* and *Adrb3*. For those genes, a Gamma distribution with a log-link was necessary to meet model assumptions.

For immunohistology of RXXpS/T, to test whether the acute treatment (vehicle or agonist) affected PKA-phosphorylation in MN and whether this effect differed between WT and SOD1 mice, a linear mixed model with genotype, treatment and their interaction as fixed effects and a per-animal random offset was calculated.

For immediate early genes and ion channels RT-qPCR, to test if the acute treatment (vehicle or agonist) affected MN mRNA expression and whether this effect differed between WT and SOD1 mice, a linear model with genotype and treatment as well as their interaction were calculated for each gene. The PCA plot for acutely treated mice was generated with Clustvis software (Metsalu and Vilo, 2015).

For GPCR ISH upon chemogenetic treatment, to test whether the chronic DREADD(Gs) activation affected MN transcription differed in infected (Gs+) or in non infected (Gs-) MNs, a generalized linear mixed model with MN type (Gs+ or Gs-) as a fixed and dispersion effect, a per-animal random offset, and a Gamma error-distribution with a log-link function were calculated for each gene.

For GPCR ISH upon adrenergic agonist treatment, to test whether the chronic treatment (vehicle or agonist) affected MN transcription, a generalized linear mixed model with treatment as a fixed and dispersion effect, a per-animal random offset, and a log-link function were calculated for each gene. For Adora2b, a Gamma error distribution was used.

For misfSOD1 immunohistology, to test whether the chronic treatment (vehicle or agonist) affected misfSOD1 levels, a generalized linear mixed model with treatment as a fixed and dispersion effect, a per-animal random offset, and a log-link function was calculated.

For electrophysiology, to test if the treatment affected intrinsic neuronal properties and whether this effect differed between WT and SOD1 mice, we calculated linear mixed models for each intrinsic parameter. Fixed effects for treatment (acute: before or after; chronic: vehicle or agonist) and genotype (WT or SOD1) as well as their interaction effect were included. To account for between animal variance, a random per-animal offset was introduced. Backwards elimination was performed on the random effect, i.e., the random offset was only included if it significantly contributed to goodness-of-fit of the model.

Data obtained from the same MNs recorded before and after the iontophoretic injection of cAMP-SP were compared using a paired t-test except for maximum firing frequency where a Wilcoxon paired test.

Model assumptions were confirmed both by visually inspecting the quantile-quantile plots and histograms, and by performing distribution, dispersion, outlier, homogeneity of variance, and quantile deviation tests using the DHARMa R package (Hartig, 2022). If model assumptions were violated, following strategies were employed. Data points were identified as outliers, if the absolute value of their residual was greater than 2 standard deviations, and removed. In case of non-normality of residuals, generalized-linear (mixed) models with link function and error distributions that did not violate model assumptions were chosen. A full-factorial dispersion model was fit in case of presence of heteroscedasticity. Degrees of freedom of linear mixed models were adjusted using the Kenward-Roger method. Linear models were fit using lm, linear mixed models using *lmer* of the *lme4* R-package (Bates *et al*., 2015), and generalized linear (mixed) models using *glmmTMB* (a Template Model Builder interface for R; Brooks *et al*., 2017). Planned post-hoc tests were performed to test if there was a significant treatment effect within WT or SOD1 mice. Throughout, an alpha-error of $p<0.05$ was regarded as significant.

## Supplementary Material

**Supplemental Table 1 | qPCR primer list.**

| Housekeeping gene | Forward primer sequence (5'-3') | Reverse primer sequence (5'-3') |
|---|---|---|
| *Gapdh* | TGGATCTGACGTGCCGC | TGCCTGCTTCACCACCTTC |

| Negative control gene | Forward primer sequence (5'-3') | Reverse primer sequence (5'-3') |
|---|---|---|
| *Gfp* | GAAGCGCGATCACATGGT | CCATGCCGAGAGTGATCC |

| GPCR-encoding genes | Forward primer sequence (5'-3') | Reverse primer sequence (5'-3') |
|---|---|---|
| *Adcyap1r1* | TATGGACTTCAAGCACCGGC | TCTTGCTCAGGATGGACAGC |
| *Adora2a* | GTTAGGTAGGCAGAGGGACAGG | CTGCGATTGCTTCCCTTCTCTG |
| *Adora2b* | GGAACCGAGACTTCCGCTAC | GACTGAGAGTAGACTGCGCC |
| *Adrb1* | CTACAACGACCCCAAGTGCT | ACGTAGAAGGAGACGACGGA |
| *Adrb2* | TACACAGGGGAGCCAAACAC | TCAACGCTAAGGCTAGGCAC |
| *Adrb3* | CAGGCTCTGTGTCTCTGGTTA | GAGGAGACAGGGATGAAACCTC |
| *Agtr1a* | CTTAGGGTTGGAACCTGCGG | TCATCCAGTCCCTCCCAACT |
| *Bdkrb1* | CCGCTACAGGTTGCTGGTAT | TTGACGGAACGCAGAAGGAA |
| *Cckar* | ACTGCCAAGTCCACGTTCAA | TCATCTGGGGCGTTCCAAAA |
| *Chrm2* | ACTGCCATTGCGGCTTTCTA | TATTCTGCTCTTGCTCGCCC |
| *Chrm4* | GCCTCTGGCTAGTTCCGCC | TCGCCATGCTGAACCCAAC |
| *Drd2* | GACACCACTCAAGGGCAACT | ATCCATTCTCCGCCTGTTCA |

| | | |
|---|---|---|
| *Drd5* | CGAACCTACGCCATCTCCTC | GCGCGTGTAGGTCACTATCA |
| *Gabbr2* | ACAGGCGATTCCAGTTCACA | CGTAGGCGGTGGTTTTCTGA |
| *Gpr3* | ATCTACGCCTTTCGCAACCA | CGGGACCGGAATGGAATCTT |
| *Gpr65* | CATGGGCTACGCAATACCCT | TGTTTTCCGTGGCTTGGTTG |
| *Gpr68* | ACGATACCAGCCCAAGTGTG | CACCTTAACCAGTCCTCTGGC |
| *Grm4* | TACCAGTACCAACGTCGCAA | GCATCCGCTCTATTCTGAGGT |
| *Grm8* | TGTGCTCCTAACGGGGATTT | GATGATTGTGTCAGGTGCCG |
| *Hcar1* | AGTGTGAAGGAAACCGTGGG | CGCTTTTCTCAGCCATGCAA |
| *Hcar2* | GCGGCCATCATTTCTTGCTT | GCCTCGCCATTTTTGGTCAT |
| *Hrh3* | TTAGAGCATCAACCCGGCAG | CACTCCAGTTCCACCAACGA |
| *Htr7* | GTGGTCAAAATGGGAAACGGA | CCATTCTGCCTCACGGGGTA |
| *Lpar2* | GGCAGATGACTTGACTTCGC | GCCTCCCTGAATGTTTGCTC |
| *Oprd1* | TGGATGCTTTTGGGGTTCCT | AAACAAAGGGTCTCGGTGCT |
| *Oprl1* | TCCTCAGGCACACCAAGATG | GAAGGGCAGTGTCAGCAAGA |
| *P2ry12* | AACGCCAGTGTCATTTGCTG | TCTCCTTTTATTCTTGCACTGTGAC |
| *Pthr1* | AGCGAGTGCCTCAAGTTCAT | TCCCACGGTGTAGATCATGC |
| *S1pr5* | AACTCGCTGCTGAATCCCAT | GGAGGAGTCTTGGTTGCAGG |
| *Tacr1* | AGGTGTCTGGGGGTTTCTTTA | CCTAGAAGTGACAGGTGACCA |

| **Immediate-early genes** | **Forward primer sequence (5’-3’)** | **Reverse primer sequence (5’-3’)** |
|---|---|---|

| | | |
|---|---|---|
| *ΔFosB* | AGGCAGAGCTGGAGTCGGAGAT | GCCGAGGACTTGAACTTCACTCG |
| *Arc* | GCACAAAAGCCATGACCCAT | TCTCCCTAGTCCCCAGGGC |
| *c-Fos* | CCTGCCCCTTCTCAACGAC | GCTCCACGTTGCTGATGCT |
| *Egr1* | GCCGAGCGAACAACCCTAT | TCCACCATCGCCTTCTCATT |
| *Egr2* | GTTGACTGTCACTCCAAGAAATGG | AGCGCAGCCCTGTAGGC |
| *NPas4* | GCTATACTCAGAAGGTCCAGAAGGC | TCAGAGAATGAGGGTAGCACAGC |

| **Ion channel-encoding genes** | **Forward primer sequence (5'-3')** | **Reverse primer sequence (5'-3')** |
|---|---|---|
| *Cacna1d* (isof.1) | GCTCGGTGGCTGTATTTTCAA | CCGTGCTTTCTACCGCACTT |
| *Cacna2d3* | GCAGATCGCAGGAAGCTTTG | ACGGGAGATTTCCGCTCATC |
| *Hcn1* | CGTGAAGCATGACCGAGAGA | GTAGACTGGCGGAGATTGGG |
| *Hcn2* | CATCCACACCAAAGCCATGC | CCCGCCTCCTAAGCTACCTA |
| *Kcna1* | TGCTGTGTGTCGCTCAATCT | TCTCCGAACTGGACACTTGC |
| *Kcna2* | TACCCATCTGCAAGGGCAACG | CGACTTGAGGAGGAGAGTGGA |
| *Kcnab1* | TCTTGGACTGGTCCCCTACC | AGATTCCCCTACCCCAGCAT |
| *Kcnb1* | GAGAGGGCGTGGCTAAGAAG | GCCCTCTTGGTCCATTTCCA |
| *Kcnj14* | GCCGAGGACAGACCTGAACAC | ACTGGGGGTTCCTCTGCTCA |
| *Kcnn3* | ATCCACCGTCATCCTGCTTG | GTAGGTCATGGCTATCCGCC |
| *Kcnn2* | ACAAGGCGTCGCTGTATTCT | CTGTATTTCCCTGGCGTGGT |

| | | |
|---|---|---|
| *Kcnq2* | GCCATTTTGTACGTGCCCTT | TAGAAGACAGCGTCGTGTGC |
| *Kcnq3* | AGTCTTGCTTCCCTGGTGATTC | TCGTCCTGCATTTGGCTGATA |
| *Kcnq5* | GCAGCCACCAGACTAAAGGA | CTGCCGCTTCCAATTCCAAA |
| *Kcnt2* | CTGTGCACTTAAAAGCAATACAGT | AGCATTTTCCACATCCATGACT |
| *Scn1a* | TACAGAAGCAGACCGTAGGC | TGTGATTAGCATCATTTTGGGCT |
| *Scn8a* | CCTTCTTACGAGACCCGTGG | ACCCTGAAAGTGCGTAGAGC |
| *Tmem16f* | TGGAACCCTGATCTTCGCTG | TTGCTGTAGCTCAACGGTGT |
| *Trpm5* | GAATGGGGACTACAGAGGCTG | CGAATGTTTCCTGTGGAGGC |

## Supplementary Figure

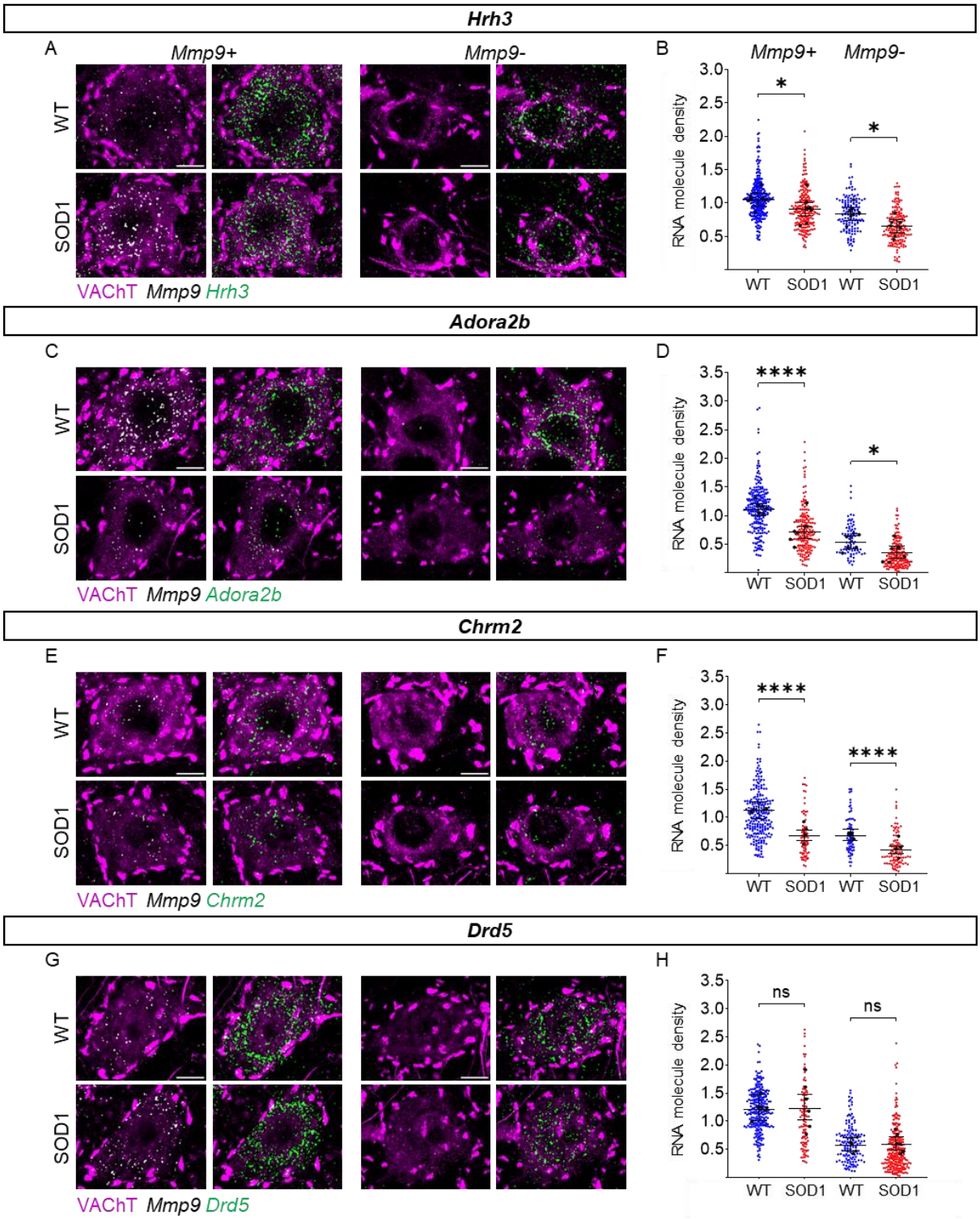


**Supplemental Figure 1 | Additional disease-driven transcriptional changes in pre-symptomatic SOD1 MNs at single-molecule single-MN resolution. A, C, E, G)** Representative confocal images of individual p45 WT and SOD1 *Mmp9+* and *Mmp9-* MNs for *Hrh3*, *Adora2b*, *Chrm2* and *Drd5* ISH, respectively. MNs are identified by VAChT+ C-boutons and diffuse cytoplasmic signal (magenta); cytoplasmic spots define single mRNA molecules of *Mmp9* (white) or the GPCRs of interest (green). Scale bar=10µm. **B, D, F, H)** Quantification of the density of single mRNA molecules of *Hrh3* **(B)**, *Adora2b* **(D),** *Chrm2* (**G**) and *Drd5* **(H)** per MN cross-section area. In each dot plot, small dots correspond to individual MN, whereas large dots indicate individual mouse means; the error bar delineates the overall mean and corresponding 95% confidence interval (for *Chrm2* and *Drd5* it is back-propagated from the log scale). N = 4-6 mice per genotype group. **p*<0.05, ***p*<0.01, ****p*<0.001, *****p*<0.0001, ns - non significant.

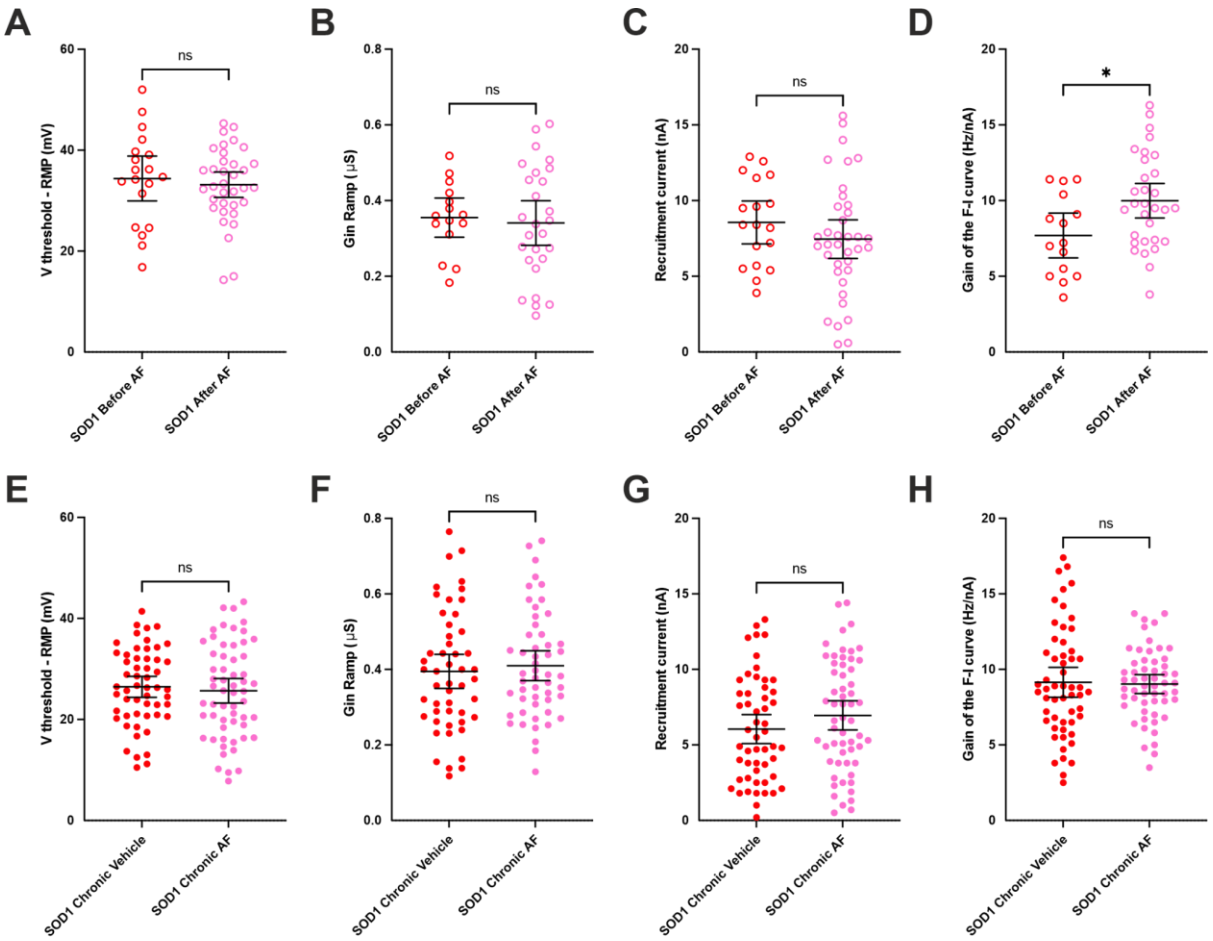


**Supplemental Figure 2 | Replication of acute and prolonged delivery of adrenergic β2/β3 agonists on a different cohort. A-H)** Electrophysiological properties were obtained from slow ramps of current, as in Figure 3 and 7 but were performed in Poznan. **A-D)** Effect of the acute treatment on Voltage threshold - resting membrane potential **(A)**, ramp input conductance **(B)**, recruitment current **(C)**, gain of the F-I relationship **(D),** in MNs from SOD1 mice. **E-H)** Effect of the chronic treatment on Voltage threshold - resting membrane potential **(E)**, ramp input conductance **(F)**, recruitment current **(G)**, gain of the F-I relationship **(H),** in MNs from SOD1 mice. In all graphs, each point represents one MN and the mean ± 95% CI are shown. Significances on top bars are for treatment effects. N =7 Acute SOD1 mice and N = 11 Chronic SOD1 mice. *$p$<0.05, **$p$<0.01, ***$p$<0.001, ****$p$<0.0001, ns - non significant.

## References


Bączyk, M., Manuel, M., Roselli, F., and Zytnicki, D. (2022). From Physiological Properties to Selective Vulnerability of Motor Units in Amyotrophic Lateral Sclerosis. Adv Neurobiol *28*, 375–394. 10.1007/978-3-031-07167-6_15.

Bączyk, M., Alami, N.O., Delestrée, N., Martinot, C., Tang, L., Commisso, B., Bayer, D., Doisne, N., Frankel, W., Manuel, M., Roselli, F., and Zytnicki, D. (2020). Synaptic restoration by cAMP/PKA drives activity-dependent neuroprotection to motoneurons in ALS. J. Exp. Med. *217*. 10.1084/jem.20191734.

Bates, D., Mächler, M., Bolker, B., and Walker, S. (2015). Fitting Linear Mixed-Effects Models Using lme4. J. Stat. Softw. *67*, 1–48. 10.18637/jss.v067.i01.

Benovic, J.L., Pike, L.J., Cerione, R.A., Staniszewski, C., Yoshimasa, T., Codina, J., Caron, M.G., and Lefkowitz, R.J. (1985). Phosphorylation of the mammalian beta-adrenergic receptor by cyclic AMP-dependent protein kinase. Regulation of the rate of receptor phosphorylation and dephosphorylation by agonist occupancy and effects on coupling of the receptor to the stimulatory guanine nucleotide regulatory protein. J. Biol. Chem. *260*, 7094–7101.

Bos, R., Drouillas, B., Bouhadfane, M., Pecchi, E., Trouplin, V., Korogod, S.M., and Brocard, F. (2021). Trpm5 channels encode bistability of spinal motoneurons and ensure motor control of hindlimbs in mice. Nat. Commun. *12*, 6815. 10.1038/s41467-021-27113-x.

Bras, H., Jankowska, E., Noga, B., and Skoog, B. (1990). Comparison of Effects of Various Types of NA and 5-HT Agonists on Transmission from Group II Muscle Afferents in the Cat. Eur. J. Neurosci. *2*, 1029–1039. 10.1111/j.1460-9568.1990.tb00015.x.

Brooks, M.E., Kristensen, K., Benthem, K.J., Magnusson, A., Berg, C.W., Nielsen, A., Skaug, H., Mächler, M., and Bolker, B. (2017). glmmTMB Balances Speed and Flexibility Among Packages for Zero-inflated Generalized Linear Mixed Modeling. R J. 10.32614/RJ-2017-066.

Catanese, A., Rajkumar, S., Sommer, D., Freisem, D., Wirth, A., Aly, A., Massa-López, D., Olivieri, A., Torelli, F., Ioannidis, V., Lipecka, J., Guerrera, I.C., Zytnicki, D., Ludolph, A.C., Kabashi, E., Mulaw, M. A., Roselli, F., and Boeckers, T.M. (2021). Synaptic disruption and CREB-regulated transcription are restored by K+ channel blockers in ALS. EMBO Mol. Med. *13*, e13131. 10.15252/emmm.202013131.

Cerda, O., and Trimmer, J.S. (2011). Activity-dependent phosphorylation of neuronal Kv2.1 potassium channels by CDK5. J. Biol. Chem. *286*, 28738–28748. 10.1074/jbc.M111.251942.

Commisso, B., Ding, L., Varadi, K., Gorges, M., Bayer, D., Boeckers, T.M., Ludolph, A.C., Kassubek, J., Müller, O.J., and Roselli, F. (2018). Stage-dependent remodeling of projections to motor cortex in ALS mouse model revealed by a new variant retrograde-AAV9. Elife *7*. 10.7554/eLife.36892.

Danner, S., Frank, M., and Lohse, M.J. (1998). Agonist regulation of human beta2-adrenergic receptor mRNA stability occurs via a specific AU-rich element. J. Biol. Chem. *273*, 3223–3229. 10.1074/jbc.273.6.3223.

Deardorff, A.S., Romer, S.H., and Fyffe, R.E.W. (2021). Location, location, location: the organization and roles of potassium channels in mammalian motoneurons. J. Physiol. *599*, 1391–1420. 10.1113/JP278675

Deardorff, A.S., Romer, S.H., Deng, Z., Bullinger, K.L., Nardelli, P., Cope, T.C., and Fyffe, R.E.W. (2013). Expression of postsynaptic Ca2+-activated K+ (SK) channels at C-bouton synapses in mammalian lumbar -motoneurons. J. Physiol. *591*, 875–897. 10.1113/jphysiol.2012.240879.

Delestrée, N., Manuel, M., Iglesias, C., Elbasiouny, S.M., Heckman, C.J., and Zytnicki, D. (2014). Adult spinal motoneurones are not hyperexcitable in a mouse model of inherited amyotrophic lateral sclerosis. J. Physiol. *592*, 1687–1703. 10.1113/jphysiol.2013.265843.

Faber, E.S.L., Delaney, A.J., Power, J.M., Sedlak, P.L., Crane, J.W., and Sah, P. (2008). Modulation of SK channel trafficking by beta adrenoceptors enhances excitatory synaptic transmission and plasticity in the amygdala. J. Neurosci. *28*, 10803–10813. 10.1523/JNEUROSCI.1796-08.2008.

Gainetdinov, R.R., Premont, R.T., Bohn, L.M., Lefkowitz, R.J., and Caron, M.G. (2004). Desensitization of G protein-coupled receptors and neuronal functions. Annu. Rev. Neurosci. *27*, 107–144. 10.1146/annurev.neuro.27.070203.144206.

Gurney, M.E., Pu, H., Chiu, A.Y., Dal Canto, M.C., Polchow, C.Y., Alexander, D.D., Caliendo, J., Hentati, A., Kwon, Y.W., and Deng, H.X. (1994). Motor neuron degeneration in mice that express a human Cu,Zn superoxide dismutase mutation. Science *264*, 1772–1775. 10.1126/science.8209258.

Hammar, I., Bannatyne, B.A., Maxwell, D.J., Edgley, S.A., and Jankowska, E. (2004). The actions of monoamines and distribution of noradrenergic and serotoninergic contacts on different subpopulations of commissural interneurons in the cat spinal cord. Eur. J. Neurosci. *19*, 1305–1316. 10.1111/j.1460-9568.2004.03239.x.

Han, P., Nakanishi, S.T., Tran, M.A., and Whelan, P.J. (2007). Dopaminergic modulation of spinal neuronal excitability. J. Neurosci. *27*, 13192–13204. 10.1523/JNEUROSCI.1279-07.2007.

Han, P., and Whelan, P.J. (2009). Modulation of AMPA currents by D(1)-like but not D(2)-like receptors in spinal motoneurons. Neuroscience *158*, 1699–1707. 10.1016/j.neuroscience.2008.11.040.

Hausdorff, W.P., Campbell, P.T., Ostrowski, J., Yu, S.S., Caron, M.G., and Lefkowitz, R.J. (1991). A small region of the beta-adrenergic receptor is selectively involved in its rapid regulation. Proc. Natl. Acad. Sci. U. S. A. *88*, 2979–2983. 10.1073/pnas.88.8.2979.

Heckman, C.J., Mottram, C., Quinlan, K., Theiss, R., and Schuster, J. (2009). Motoneuron excitability: the importance of neuromodulatory inputs. Clin. Neurophysiol. *120*, 2040–2054. 10.1016/j.clinph.2009.08.009.

Henry, A.M., and Hohmann, J.G. (2012). High-resolution gene expression atlases for adult and developing mouse brain and spinal cord. Mamm. Genome *23*, 539–549. 10.1007/s00335-012-9406-2.

Huang, B., Li, Y., Cheng, D., He, G., Liu, X., and Ma, L. (2018). β-Arrestin-biased β-adrenergic signaling promotes extinction learning of cocaine reward memory. Sci. Signal. *11*. 10.1126/scisignal.aam5402.

Ito, M., and Oshima, T. (1965). Electrical behaviour of the motoneurone membrane during intracellularly applied current steps. J. Physiol. *180*, 607–635. 10.1113/jphysiol.1965.sp007720.

Jordan, L.M., Liu, J., Hedlund, P.B., Akay, T., and Pearson, K.G. (2008). Descending command systems for the initiation of locomotion in mammals. Brain Res. Rev. *57*, 183–191. 10.1016/j.brainresrev.2007.07.019.

Kanning, K.C., Kaplan, A., and Henderson, C.E. (2010). Motor neuron diversity in development and disease. Annu. Rev. Neurosci. *33*, 409–440. 10.1146/annurev.neuro.051508.135722.

Kaplan, A., Spiller, K.J., Towne, C., Kanning, K.C., Choe, G.T., Geber, A., Akay, T., Aebischer, P., and Henderson, C.E. (2014). Neuronal matrix metalloproteinase-9 is a determinant of selective neurodegeneration. Neuron *81*, 333–348. 10.1016/j.neuron.2013.12.009

Kernell, D. (1999). Repetitive impulse firing in motoneurons: facts and perspectives. Prog. Brain Res. *123*, 31–37. 10.1016/s0079-6123(08)62841-1.

Khosravi, B., LaClair, K.D., Riemenschneider, H., Zhou, Q., Frottin, F., Mareljic, N., Czuppa, M., Farny, D., Hartmann, H., Michaelsen, M., Arzberger, T., Hartl, F.U., Hipp, M.S., and Edbauer, D. (2020). Cell-to-cell transmission of C9orf72 poly-(Gly-Ala) triggers key features of ALS/FTD. EMBO J. *39*, e102811. 10.15252/embj.2019102811.

Lefkowitz, R.J., Rockman, H.A., and Koch, W.J. (2000). Catecholamines, cardiac beta-adrenergic receptors, and heart failure. Circulation *101*, 1634–1637. 10.1161/01.cir.101.14.1634.

Leroy, F., Lamotte d'Incamps, B., Imhoff-Manuel, R.D., and Zytnicki, D. (2014). Early intrinsic hyperexcitability does not contribute to motoneuron degeneration in amyotrophic lateral sclerosis. Elife *3*. 10.7554/eLife.04046.

Lohse, M.J., Engelhardt, S., and Eschenhagen, T. (2003). What is the role of beta-adrenergic signaling in heart failure? Circ. Res. *93*, 896–906. 10.1161/01.RES.0000102042.83024.CA.

Manuel, M., Iglesias, C., Donnet, M., Leroy, F., Heckman, C.J., and Zytnicki, D. (2009). Fast kinetics, high-frequency oscillations, and subprimary firing range in adult mouse spinal motoneurons. J. Neurosci. *29*, 11246–11256. 10.1523/JNEUROSCI.3260-09.2009.

Manuel, M., Meunier, C., Donnet, M., and Zytnicki, D. (2006). The afterhyperpolarization conductance exerts the same control over the gain and variability of motoneurone firing in anaesthetized cats. J. Physiol. *576*, 873–886. 10.1113/jphysiol.2006.117002.

Maratta, R., Fenrich, K.K., Zhao, E., Neuber-Hess, M.S., and Rose, P.K. (2015). Distribution and density of contacts from noradrenergic and serotonergic boutons on the dendrites of neck flexor motoneurons in the adult cat. J. Comp. Neurol. *523*, 1701–1716. 10.1002/cne.23765.

Martínez-Silva, M. de L., Imhoff-Manuel, R.D., Sharma, A., Heckman, C.J., Shneider, N.A., Roselli, F.,Zytnicki, D., and Manuel, M. (2018). Hypoexcitability precedes denervation in the large fast-contracting motor units in two unrelated mouse models of ALS. Elife *7*, e30955. 10.7554/eLife.30955.

McLarnon, J.G. (1995). Potassium currents in motoneurones. Prog. Neurobiol. *47*, 513–531. 10.1016/0301-0082(95)00032-1.

Matera, M.G., Page, C.P., Calzetta, L., Rogliani, P., and Cazzola, M. (2020). Pharmacology and Therapeutics of Bronchodilators Revisited. Pharmacol. Rev. *72*, 218–252. 10.1124/pr.119.018150.

Metsalu, T., and Vilo, J. (2015). ClustVis: a web tool for visualizing clustering of multivariate data using Principal Component Analysis and heatmap. Nucleic Acids Res. *43*, W566–W570. 10.1093/nar/gkv468.

Meunier, C., and Borejsza, K. (2005). How membrane properties shape the discharge of motoneurons: a detailed analytical study. Neural Comput. *17*, 2383–2420. 10.1162/0899766054796923.

Michel, L.Y.M., and Balligand, J.-L. (2017). New and Emerging Therapies and Targets: Beta-3 Agonists. Handb. Exp. Pharmacol. *243*, 205–223. 10.1007/164_2016_88.

Milano, S., Gerbino, A., Schena, G., Carmosino, M., Svelto, M., and Procino, G. (2018). Human β3-Adrenoreceptor is Resistant to Agonist-Induced Desensitization in Renal Epithelial Cells. Cell. Physiol. Biochem. *48*, 847–862. 10.1159/000491916.

Miles, G.B., Hartley, R., Todd, A.J., and Brownstone, R.M. (2007). Spinal cholinergic interneurons regulate the excitability of motoneurons during locomotion. Proc. Natl. Acad. Sci. U. S. A. *104*, 2448–2453. 10.1073/pnas.0611134104.

Montague, S.J., Fenrich, K.K., Mayer-Macaulay, C., Maratta, R., Neuber-Hess, M.S., and Rose, P.K. (2013). Nonuniform distribution of contacts from noradrenergic and serotonergic boutons on the dendrites of cat splenius motoneurons. J. Comp. Neurol. *521*, 638–656. 10.1002/cne.23196.

Nascimento, F., Broadhead, M.J., Tetringa, E., Tsape, E., Zagoraiou, L., and Miles, G.B. (2020). Synaptic mechanisms underlying modulation of locomotor-related motoneuron output by premotor cholinergic interneurons. Elife *9*. 10.7554/eLife.54170.

Nicholas, A.P., Hökfelt, T., and Pieribone, V.A. (1996). The distribution and significance of CNS adrenoceptors examined with in situ hybridization. Trends Pharmacol. Sci. *17*, 245–255. 10.1016/0165-6147(96)10022-5.

Nielsen, J.B., Crone, C., and Hultborn, H. (2007). The spinal pathophysiology of spasticity--from a basic science point of view. Acta Physiol. *189*, 171–180. 10.1111/j.1748-1716.2006.01652.x.

olde Heuvel, F., Holl, S., Chandrasekar, A., Li, Z., Wang, Y., Rehman, R., Förstner, P., Sinske, D., Palmer, A., Wiesner, D., Ludolph, A.C., Huber-Lang, M., Relja, B., Wirth, T., Roeszer, T., Baumann, B., Boeckers, T.M., Knoell, B., and Roselli, F. (2019). STAT6 mediates the effect of ethanol on neuroinflammatory response in TBI. Brain Behav. Immun. *81*, 228–246. 10.1016/j.bbi.2019.06.019.

Ouali Alami, N., Schurr, C., Olde Heuvel, F., Tang, L., Li, Q., Tasdogan, A., Kimbara, A., Nettekoven, M., Ottaviani, G., Raposo, C., Roever, S., Rogers-Evans, M., Rotenhaeulser, B., Ullmer, C., Fingerle, J., Grether, U., Knuesel, I., Boeckers, T.M., Ludolph, A.C., Wirth, T., Roselli, F., and Baumann, B. (2018). NF-κB activation in astrocytes drives a stage-specific beneficial neuroimmunological response in ALS. EMBO J. *37*. 10.15252/embj.201798697.

Perrier, J.-F. (2019). If serotonin does not exhaust you, it makes you stronger. J. Physiol. *597*, 5–6. 10.1113/JP277317.

Rekling, J.C., Funk, G.D., Bayliss, D.A., Dong, X.W., and Feldman, J.L. (2000). Synaptic control of motoneuronal excitability. Physiol. Rev. 80, 767–852. 10.1152/physrev.2000.80.2.767.

Ren, Y., Barnwell, L.F., Alexander, J.C., Lubin, F.D., Adelman, J.P., Pfaffinger, P.J., Schrader, L.A., and Anderson, A.E. (2006). Regulation of surface localization of the small conductance Ca2+-activated potassium channel, Sk2, through direct phosphorylation by cAMP-dependent protein kinase. J. Biol. Chem. *281*, 11769–11779. 10.1074/jbc.M513125200.

Romer, S.H., Deardorff, A.S., and Fyffe, R.E.W. (2019). A molecular rheostat: Kv2.1 currents maintain or suppress repetitive firing in motoneurons. J. Physiol. *597*, 3769–3786. 10.1113/JP277833.

Rossi, J., Balthasar, N., Olson, D., Scott, M., Berglund, E., Lee, C.E., Choi, M.J., Lauzon, D., Lowell, B.B., and Elmquist, J.K. (2011). Melanocortin-4 receptors expressed by cholinergic neurons regulate energy balance and glucose homeostasis. Cell Metab. *13*, 195–204. 10.1016/j.cmet.2011.01.010.

Saxena, S., Roselli, F., Singh, K., Leptien, K., Julien, J.-P., Gros-Louis, F., and Caroni, P. (2013). Neuroprotection through excitability and mTOR required in ALS motoneurons to delay disease and extend survival. Neuron *80*, 80–96. 10.1016/j.neuron.2013.07.027.

Schindelin, J., Arganda-Carreras, I., Frise, E., Kaynig, V., Longair, M., Pietzsch, T., Preibisch, S., Rueden, C., Saalfeld, S., Schmid, B., Tinivez, J.-Y., White, D.J., Hartenstein, V., Eliceiri, K., Tomancak, P., and Cardona, A.. (2012). Fiji: an open-source platform for biological-image analysis. Nat. Methods *9*, 676–682. 10.1038/nmeth.2019.

Song, J., Dikwella, N., Sinske, D., Roselli, F., and Knöll, B. (2023). SRF deletion results in earlier disease onset in a mouse model of amyotrophic lateral sclerosis. JCI Insight *8*. 10.1172/jci.insight.167694.

Soulard, C., Salsac, C., Mouzat, K., Hilaire, C., Roussel, J., Mezghrani, A., Lumbroso, S., Raoul, C., and Scamps, F. (2020). Spinal Motoneuron TMEM16F Acts at C-boutons to Modulate Motor Resistance and Contributes to ALS Pathogenesis. Cell Rep. *30*, 2581–2593.e7. 10.1016/j.celrep.2020.02.001.

Takahashi, T. (1990). Inward rectification in neonatal rat spinal motoneurones. J. Physiol. *423*, 47–62. 10.1113/jphysiol.1990.sp018010.

Tartas, M., Morin, F., Barrière, G., Goillandeau, M., Lacaille, J.-C., Cazalets, J.-R., and Bertrand, S.S. (2010). Noradrenergic modulation of intrinsic and synaptic properties of lumbar motoneurons in the neonatal rat spinal cord. Front. Neural Circuits *4*, 4. 10.3389/neuro.04.004.2010.

Tinevez, J.-Y., Perry, N., Schindelin, J., Hoopes, G.M., Reynolds, G.D., Laplantine, E., Bednarek, S.Y., Shorte, S.L., and Eliceiri, K.W. (2017). TrackMate: An open and extensible platform for single-particle tracking. Methods *115*, 80–90. 10.1016/j.ymeth.2016.09.016.

Tran, T.M., Friedman, J., Qunaibi, E., Baameur, F., Moore, R.H., and Clark, R.B. (2004). Characterization of agonist stimulation of cAMP-dependent protein kinase and G protein-coupled receptor kinase phosphorylation of the beta2-adrenergic receptor using phosphoserine-specific antibodies. Mol. Pharmacol. *65*, 196–206. 10.1124/mol.65.1.196.

Trojsi, F., D'Alvano, G., Bonavita, S., and Tedeschi, G. (2020). Genetics and Sex in the Pathogenesis of Amyotrophic Lateral Sclerosis (ALS): Is There a Link? Int. J. Mol. Sci. *21*. 10.3390/ijms21103647.

Wachter, S.B., and Gilbert, E.M. (2012). Beta-adrenergic receptors, from their discovery and characterization through their manipulation to beneficial clinical application. Cardiology *122*, 104–112. 10.1159/000339271.

Wang, J., Hanada, K., Staus, D.P., Makara, M.A., Dahal, G.R., Chen, Q., Ahles, A., Engelhardt, S., and Rockman, H.A. (2017). Gαi is required for carvedilol-induced β1 adrenergic receptor β-arrestin biased signaling. Nat. Commun. *8*, 1706. 10.1038/s41467-017-01855-z.

Wang, F., Flanagan, J., Su, N., Wang, L.-C., Bui, S., Nielson, A., Wu, X., Vo, H.-T., Ma, X.-J., and Luo, Y. (2012). RNAscope: a novel in situ RNA analysis platform for formalin-fixed, paraffin-embedded tissues. J. Mol. Diagn. *14*, 22–29. 10.1016/j.jmoldx.2011.08.002.

Ye, J., Coulouris, G., Zaretskaya, I., Cutcutache, I., Rozen, S., and Madden, T.L. (2012). Primer-BLAST: a tool to design target-specific primers for polymerase chain reaction. BMC Bioinformatics *13*, 134. 10.1186/1471-2105-13-134.

Zhang, L., and Krnjević, K. (1987). Apamin depresses selectively the after-hyperpolarization of cat spinal motoneurons. Neurosci. Lett. *74*, 58–62. 10.1016/0304-3940(87)90051-6.